RESOURCE/METHODOLOGY

Systematic bromodomain protein screens identify homologous recombination and R-loop suppression pathways involved in genome integrity

Jae Jin Kim,[1,2,9] Seo Yun Lee,[1,2,9] Fade Gong,[1,2,8] Anna M. Battenhouse,[1,2,3] Daniel R. Boutz,[1,2,3] Aarti Bashyal,[4] Samantha T. Refvik,[1,2,5] Cheng-Ming Chiang,[6] Blerta Xhemalce,[1,2,7] Tanya T. Paull,[1,2,5,7] Jennifer S. Brodbelt,[4,7] Edward M. Marcotte,[1,2,3] and Kyle M. Miller[1,2,7]

[1]Department of Molecular Biosciences, [2]Institute for Cellular and Molecular Biology, [3]Center for Systems and Synthetic Biology, [4]Department of Chemistry, The University of Texas at Austin, Austin, Texas 78712, USA; [5]The Howard Hughes Medical Institute; [6]Simmons Comprehensive Cancer Center, Department of Biochemistry, Department of Pharmacology, University of Texas Southwestern Medical Center, Dallas, Texas 75390, USA; [7]Livestrong Cancer Institutes, Dell Medical School, The University of Texas at Austin, Austin, Texas 78712, USA

Bromodomain proteins (BRD) are key chromatin regulators of genome function and stability as well as therapeutic targets in cancer. Here, we systematically delineate the contribution of human BRD proteins for genome stability and DNA double-strand break (DSB) repair using several cell-based assays and proteomic interaction network analysis. Applying these approaches, we identify 24 of the 42 BRD proteins as promoters of DNA repair and/or genome integrity. We identified a BRD-reader function of PCAF that bound TIP60-mediated histone acetylations at DSBs to recruit a DUB complex to deubiquitylate histone H2BK120, to allowing direct acetylation by PCAF, and repair of DSBs by homologous recombination. We also discovered the bromo-and-extra-terminal (BET) BRD proteins, BRD2 and BRD4, as negative regulators of transcription-associated RNA-DNA hybrids (R-loops) as inhibition of BRD2 or BRD4 increased R-loop formation, which generated DSBs. These breaks were reliant on topoisomerase II, and BRD2 directly bound and activated topoisomerase I, a known restrainer of R-loops. Thus, comprehensive interactome and functional profiling of BRD proteins revealed new homologous recombination and genome stability pathways, providing a framework to understand genome maintenance by BRD proteins and the effects of their pharmacological inhibition.

Preserving the integrity of the genome is paramount for maintaining cellular and organismal homeostasis. In eukaryotes, the nuclear genome is organized into chromatin, which participates in compacting the genome and regulating its accessibility to promote cell identity and function. Given the constant bombardment of DNA by exogenous and endogenous factors including radiation, carcinogens, reactive oxygen species, replication stress, and dysregulated protein products (Jackson and Bartek 2009; Tubbs

and Nussenzweig 2017; Xia et al. 2019), cells engage specialized signaling pathways termed the DNA damage response (DDR) that detect, signal, and repair DNA lesions (Jackson and Bartek 2009; Ciccia and Elledge 2010). DNA double-strand breaks (DSBs) are a particularly deleterious form of DNA damage, which can provoke genome instability including insertions, deletions, translocations, and chromosome loss. DSBs are repaired by two main pathways in mammalian cells, homologous

[8]Present address: Department of Biochemistry and Molecular Biology, Baylor College of Medicine, Houston, TX 77030, USA
[9]These authors contributed equally to this work.
Corresponding author: kyle.miller@austin.utexas.edu
Article is online at http://www.genesdev.org/cgi/doi/10.1101/gad.331231.119.

recombination (HR) and classical nonhomologous end-joining (NHEJ). The importance of DDR pathways is highlighted by the various diseases associated with DDR defects, including neurodegenerative disorders, immune deficiencies, and cancer (Jackson and Bartek 2009; Negrini et al. 2010).

DNA damage and the responses and activities elicited by it are carried out within the context of chromatin. These chromatin-based DDR pathways ensure the coordination of other DNA-templated processes such as transcription and replication with the signaling and repair of DNA damage, including DSBs (Lukas et al. 2011; Polo and Jackson 2011; Miller and Jackson 2012; Gong and Miller 2013; Jackson and Durocher 2013; Agarwal and Miller 2016; Gong et al. 2016; Kim et al. 2019). For example, the histone variant H2AX is phosphorylated by ATM and DNA-PK at DSBs, which promotes the accumulation of DDR factors into microscopically visible foci at break sites including the DDR factors 53BP1 and BRCA1 (Polo and Jackson 2011; Scully and Xie 2013). 53BP1 is a multivalent chromatin interacting protein that binds to ubiquitylated histone H2A and methylated H4, while BRCA1 interacts with the nucleosome to promote its ubiquitylation activity on H2A (Fradet-Turcotte et al. 2013; Panier and Boulton 2014; Densham and Morris 2017). Chromatin plays an essential role in the DDR and in DSB signaling and repair.

Acetylation represents a key posttranslational modification that regulates chromatin structure and function, including in the DDR (Gong et al. 2016; Fujisawa and Filippakopoulos 2017). Acetylation is catalyzed by histone acetyltransferases (HATs) (Lee and Workman 2007; Verdin and Ott 2015) and erased by histone deacetylases (HDACs), (Seto and Yoshida 2014), which dynamically regulate this mark on both histone and nonhistone proteins. Acetylated lysines are recognized by multiple recognition reader domains, including the bromodomain (BRD), which is found in 42 human proteins that play key functions in chromatin regulation, including transcription and chromatin remodeling (Filippakopoulos and Knapp 2012; Filippakopoulos et al. 2012; Gong et al. 2016; Fujisawa and Filippakopoulos 2017). Over one-third of human BRD proteins and half of all human HAT and HDAC enzymes are dynamically relocalized, following DNA damage, including to the sites of DNA lesions and repair (Miller et al. 2010; Gong and Miller 2013; Gong et al. 2015). These studies from our lab and others have established the importance of acetylation signaling in the DDR (Gong et al. 2016). For example, a variant of the bromo-and-extra-terminal (BET) BRD protein BRD4 has been shown to insulate DNA damage signaling, and the BRD protein ZMYND8 recruits the NuRD chromatin remodeling complex to DNA damage sites where it promotes repression of transcription and HR repair (Floyd et al. 2013; Gong et al. 2015). Given the demonstrated role of BRD proteins in transcription and the growing evidence for their participation in the DDR, these proteins are likely to represent key mediators of transcription-associated DNA damage response pathways, although their participation and function in the DDR are not yet defined.

BRD proteins are highly mutated and/or aberrantly expressed in cancer, which has motivated targeting BRD proteins therapeutically (Muller et al. 2011; Barbieri et al. 2013; Zhang et al. 2015). These efforts are highlighted by the development and use of BET inhibitors, including JQ1 and I-BET (Filippakopoulos et al. 2010; Dawson et al. 2011), which are widely used in preclinical and clinical studies as therapeutic strategies to target various cancers (Boi et al. 2015; Andrieu et al. 2016). Given the dual functions of BRD proteins in the DDR and cancer, understanding mechanistically how BRD proteins promote genome stability, a feature often lost in cancer (Negrini et al. 2010), will be critical for revealing the involvement of BRD proteins in cancer as well as for guiding the use of cancer therapies targeting BRD proteins. As a means to address this question, we have systematically analyzed the involvement of all ubiquitously expressed human BRD proteins in promoting genome stability using diverse experimental approaches. We find that the deficiency of the majority of BRD proteins results in chromosome instability, reduced DNA damage tolerance, and DNA DSB repair defects, especially in HR repair. These data and our construction of BRD protein interactomes provided pivotal insights that led directly to the identification of two new genome integrity pathways by BRD proteins described here. We found that the HAT PCAF and an associated DUB complex localize to DNA damage sites, where PCAF engages TIP60 acetylated histones with its BRD to trigger a ubiquitin-acetylation switch on histone H2B that promotes HR repair. We further show that BRD2 or BRD4 deficiency, either by depletion using siRNAs or targeting with the small molecule Pan-BET BRD inhibitor JQ1, results in aberrant transcription and control of topological topoisomerase enzymes and R-loop formation, resulting in DSBs. Collectively, these data reveal BRD proteins as key chromatin reader proteins that are vital for maintaining the integrity of the genome through repair and transcriptional responses.

Results

Systematic identification of bromodomain proteins involved in the DNA damage response

BRD proteins are key epigenetic regulators, one-third of which we previously identified as being relocalized to DNA damage after laser-induced DNA damage (Fig. 1A; Gong et al. 2015). To further investigate the role of BRD proteins in DSB repair, we performed a siRNA screen of all BRD proteins that are widely expressed in cells using well-established HR and NHEJ cell-based reporter systems (Fig. 1B; Supplemental Fig. S1B; Pierce et al. 1999; Bennardo et al. 2008). Knockdown efficiencies of individual BRD genes by siRNAs pools were validated by RT-qPCR analyses (Supplemental Fig. S1A). The depletion of CtIP and Ligase 4, which are known regulators of HR and NHEJ, respectively, were used as positive controls for each assay. This screen identified 19 BRD genes whose depletion reduced HR >25% below HR levels observed in control cells, while NHEJ rates were comparable to
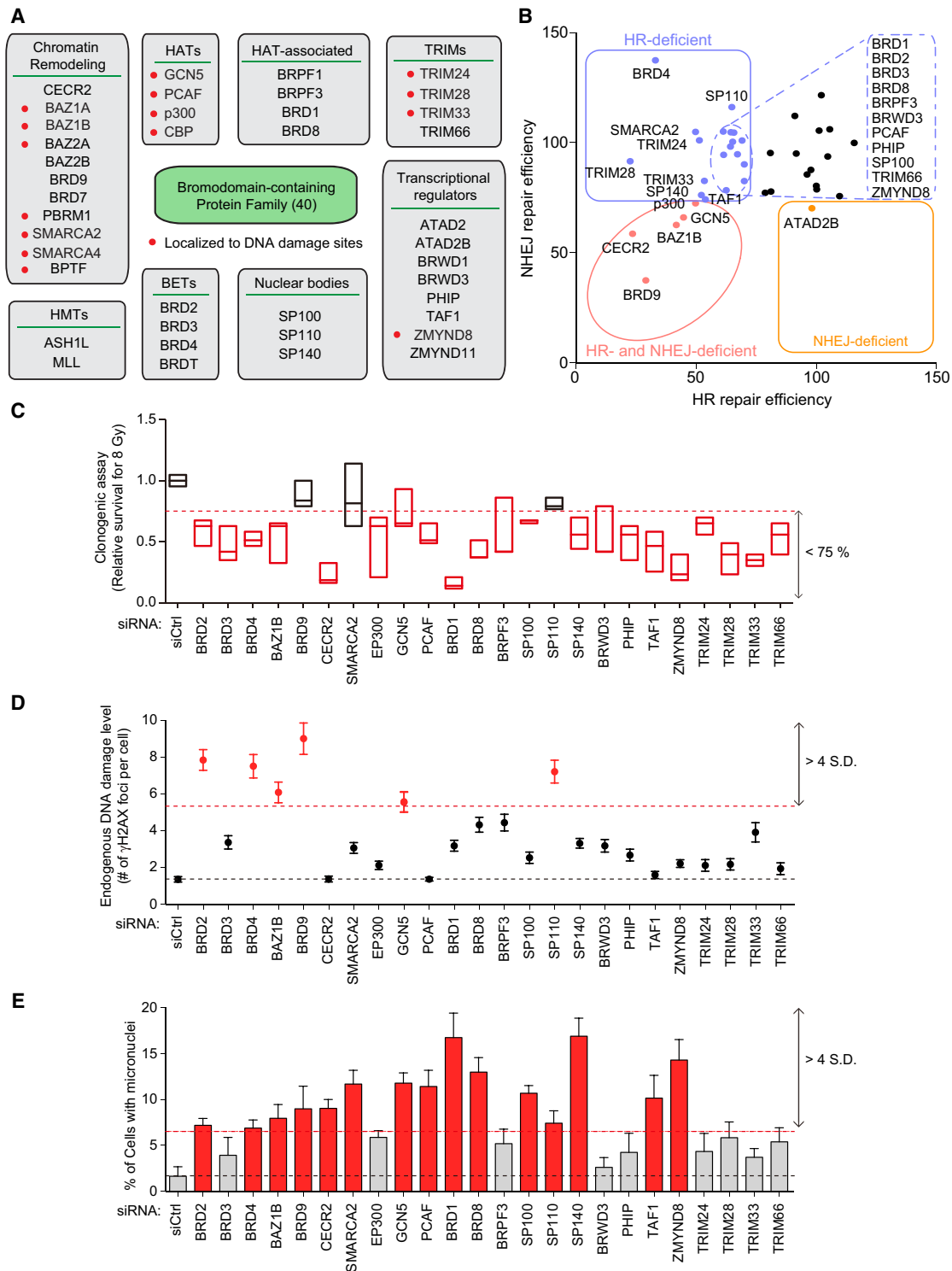
Figure 1. Human BRD proteins promote DNA double-strand break repair and genome stability. (*A*) Functional classification of human BRD proteins into eight subfamilies. DNA damage-associated BRD proteins indicated with red circle. (*B*) Comparative analysis of HR and NHEJ repair in cells deficient for each individual BRD protein. Individual BRD genes were depleted with siRNAs and analyzed for DSB repair in U2OS cells containing HR (DR) and NHEJ (EJ5) reporters. Data represent the mean of three independent experiments. (*C*) Ionizing radiation sensitivity screen for BRD proteins. Clonogenic survival assays were performed on siRNA-depleted BRD proteins that scored HR-deficient in *B*. Data shown is the ratio of relative survival for 8 Gy from three biologically independent experiments and represent the mean ± SEM. Results were normalized to control, nontargeting siRNA (siCtrl) treated cells and <75% of control values are indicated in red. (*D*) Endogenous DNA damage screen for BRD proteins. BRD proteins were depleted by siRNAs as in *C* and analyzed by immuno-fluorescence for the DNA damage marker γH2AX. BRD-deficient cells exhibiting an increase of γH2AX foci >4 standard deviations of siCtrl (4 SDs) are labeled in red. Data represent mean ± SEM from >100 cells. (*E*) BRD-deficient cells exhibit chromosome mis-segregation. Individual BRD proteins were depleted as in *B*, and cells were analyzed for micronuclei formation (see Materials and methods). An increase of >4 SDs of siCtrl are marked in red. Data represent the mean ± SEM from >100 cells.

control cells (Fig. 1B; Supplemental Fig. S1B,C). Five BRD genes, p300, GCN5, BAZ1B, CECR2, and BRD9, were required for efficient repair by both HR and NHEJ DSB repair pathways, and one gene, ATAD2B, promoted NHEJ repair only (Fig. 1B; Supplemental Fig. S1C). Our results suggest that the majority of BRD proteins (24 out of 40) are involved in DSB repair and moreover, with a noted penchant for HR repair. To further ascertain the functional involvement of BRD proteins in DSB repair, we tested the involvement of HR-promoting BRD genes in radiosensitivity, as repair-deficient cells often exhibit sensitivity to ionizing radiation (IR), a treatment that generates DSBs. Indeed, individual depletion of the 24 BRD proteins implicated in HR repair from our initial screen resulted in hypersensitivity to IR for 21 out of the 24 BRD proteins tested, supporting the notion that our reporter screen effectively identified DSB repair-promoting BRD proteins (Fig. 1C; Supplemental Fig. S2A). While several BRD proteins had previously been shown to be recruited to DNA damage sites, many HR-promoting BRD proteins from our screen have not been identified as damage-localized proteins. Due to the chromatin-bound nature of BRD proteins, their accumulation at DNA damage sites may be difficult to detect. Alternatively, these BRD proteins may promote HR independently from active association to DNA lesions through their roles in other biological processes, such as transcription, which regulate HR either directly or indirectly.

To further investigate the involvement of BRD proteins in suppressing endogenous DNA damage, we analyzed the levels of γH2AX, a marker of DSBs, in BRD-deficient cells that displayed reduced HR repair when depleted (see Fig. 1B). Compared to control cells, depletion of several BRD proteins, including BRD2, BRD4, BAZ1B, BRD9, GCN5, and SP110, significantly increased endogenous DNA damage (Fig. 1D; Supplemental Fig. S2B). Chromosomal missegregation, including the formation of micronuclei, is also indicative of defective DNA repair and endogenous DNA damage (Fenech et al. 2011). Following depletion of BRD proteins by siRNA, we monitored micronuclei formation in these cells under normal growth conditions. Consistent with defective DNA repair, radiation sensitivity, and increased levels of γH2AX that we observed upon depletion of several individual BRD proteins, the majority of BRD proteins were found to be required to suppress micronuclei formation compared to their control counterparts (Fig. 1E). Collectively, these screening results provide evidence for the involvement of BRD proteins in promoting DSB repair and genome stability.

Human BRD protein network

To investigate how individual human BRD proteins that scored as HR repair defective in our screens regulate genome integrity, we identified the human BRD protein network using a systematic proteomic approach (Fig. 2A). The interactomes of BRD proteins were obtained by analyzing affinity purification of BRD proteins coupled with mass spectrometry (AP-MS) using protocols optimized for detecting protein-protein interactions (Fig. 2A; see Ma-

terials and methods). We generated stable HEK-293 Flp-In T-REx cells, inducibly expressing individual S protein, Flag tag, Streptavidin Binding peptide (SFB)-tagged BRD proteins (baits) upon tetracycline treatment. We performed tandem affinity purification (TAP) with the 24 HR promoting BRD proteins identified in our DSB repair screen. Two biological replicates were analyzed by liquid chromatography (LC) tandem MS/MS for each bait BRD protein, as well as several controls (Supplemental Table S1). The LC-MS/MS data we obtained was searched against the human UniProt database, and peptide spectral counts were assigned to proteins (see Materials and methods). To efficiently discriminate confident interacting protein from false-positive or contaminant proteins, the probability of a bona fide protein–protein interaction was analyzed using Significance Analysis of INTeractome software (SAINTexpress) (Teo et al. 2014). Interacting proteins with a false discovery rate (FDR) <1% were further filtered to identify high-confidence interacting proteins (see Materials and methods), resulting in a total of 1109 high-confidence bait-associated proteins (i.e., preys) involved in 1805 BRD protein candidate bait/prey interactions (Supplemental Table S2). To visualize the organization of HR-regulated BRD protein interactomes, we built the protein interaction network with BRD baits and preys (Fig. 2B). This analysis revealed extensive connectivity between different BRD proteins, which may in part explain their shared involvement in HR repair and genome integrity pathways.

Our BRD protein interaction network pinpointed several complexes of immediate interest. The BRD-containing HAT proteins PCAF (KAT2B) and GCN5 (KAT2A) are components of the SAGA chromatin remodeling complex. Our AP-MS analysis revealed that the SAGA complex proteins were interacting proteins of PCAF and GCN5, suggesting that proteins within the SAGA complex may participate in HR repair processes (Fig. 2B,C). The BET BRD protein family, including BRD2, BRD3, and BRD4, is implicated in transcription regulation and cancer development (Wu and Chiang 2007; Fujisawa and Filippakopoulos 2017). Our analysis identified several transcription-associated factors and chromatin remodelers that interacted with BET proteins (Fig. 2B,D), which is in line with a recent analysis of BET BRD protein interactions (Lambert et al. 2019). Comparisons of these data sets revealed an overall overlap of 21%, with many of our high-confidence interactors observed in both studies, including TOP1 (Supplemental Table S2), a gene we validated and studied further (see below). These data sets provide high-confidence BET BRD protein interactors obtained from both studies, as well as highlight the complementary nature of these proteomic data sets obtained using different experimental approaches. We next chose to investigate further several of these protein networks with the goal of establishing how these BRD proteins function in HR repair and genome maintenance pathways. Furthermore, our results provide a HR repair-based BRD protein network, enabling a platform for future identification of BRD protein functions in genome integrity, including homologous recombination repair.
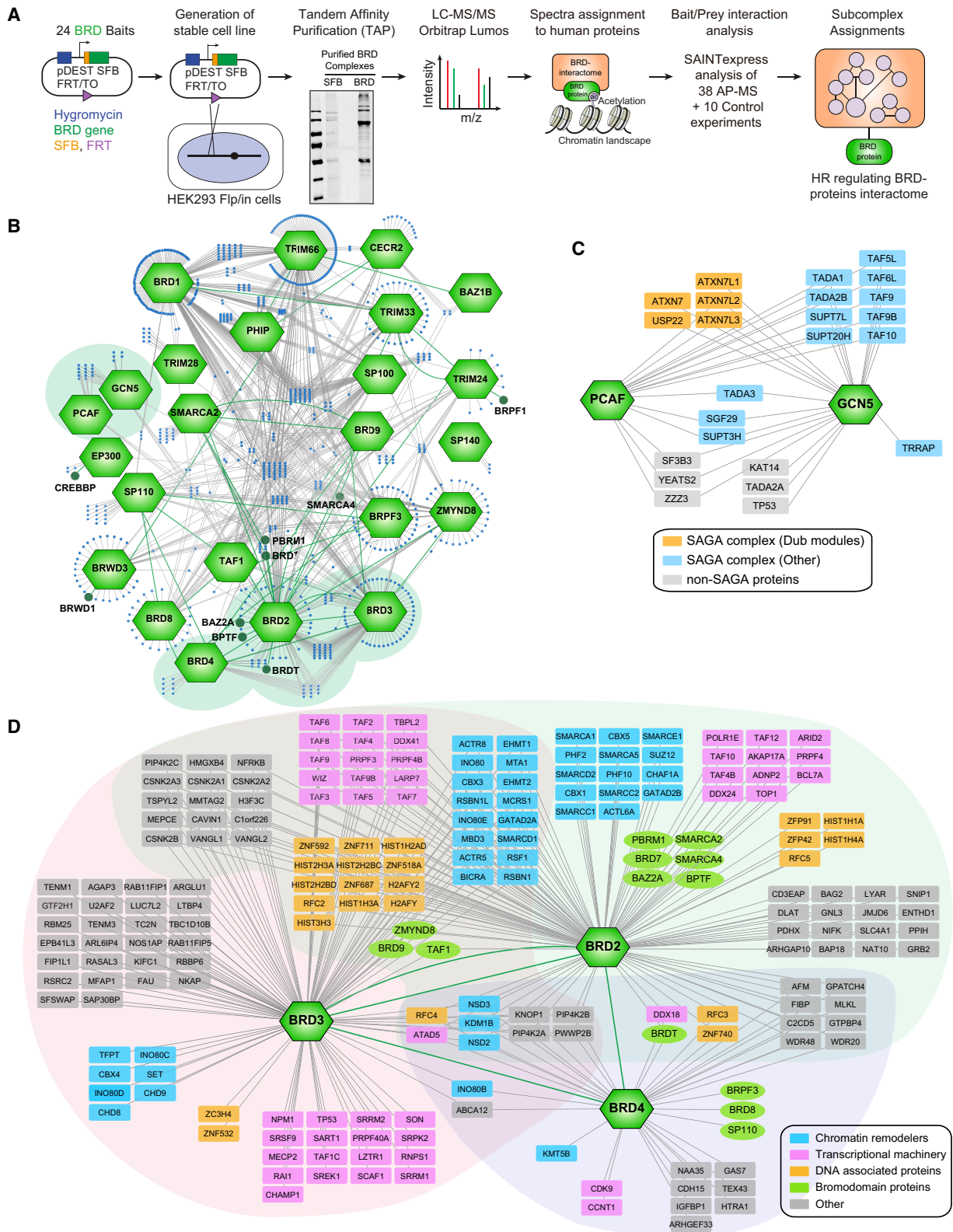
Figure 2. Protein interactome network of human BRD proteins. (*A*) Schematic overview of approach to identify protein-protein interactome of BRD proteins involved in HR repair. (*B*) Network of HR-promoting BRD proteins. Green hexagon-shaped nodes correspond to BRD-baits and blue circles indicate prey proteins. Gray lines indicate bait-prey interactions and green lines indicate BRD-BRD protein interactions. Green circles indicate BRD proteins (prey) identified as bait-prey interactions. (*C,D*) Subnetworks of GCN5/PCAF HAT-BRD and BET proteins. BRD bait and prey proteins are indicated as in *B*. For prey protein interactions, gene names are provided and placed into several categories as described in the legends. SAGA complex components are based on CORUM (Giurgiu et al. 2019) complex ID 6643 and ComplexPortal (Meldal et al. 2015) complexes CPX-900 and CPX-656. Individual BET BRD protein interactomes are shaded (BRD2: green; BRD4: purple; BRD3: pink).

The histone acetyltransferase PCAF is a DNA damage response factor

Our initial screen identified the histone acetyltransferase (HAT) PCAF as a regulator of HR repair. In addition to acetylating histones, PCAF has been linked to BRCA1 and RPA1 acetylation following UV damage and BRCA1 K830 acetylation in response to ionizing radiation (Zhao et al. 2017; Lahusen et al. 2018), but the role of PCAF in DSB repair is unknown. To validate our siRNA results, we generated PCAF knockout (KO) cell lines by CRISPR/Cas9 genome editing (Fig. 3A). We then analyzed survival following DNA damage and HR repair efficiency in two independent PCAF KO clones compared to parental cells. Loss of PCAF rendered cells sensitive to several DNA damaging agents, including IR, hydroxyurea (HU), and camptothecin (CPT), which was consistent with our initial screen results (Fig. 3A; Supplemental Fig. S3A,B). PCAF KO cells also exhibited increased levels of DSBs following these treatments compared to control cells as measured by a neutral comet assay (Fig. 3B; Supplemental Fig. S3C,D). These data were consistent with defective DNA repair resulting from PCAF deficiency. To further address this idea, HR repair of DSBs was directly measured in control and PCAF KO cells using both CRISPR-EGFP and CRISPR-mClover assays to measure HR efficiency. The CRISPR-EGFP and -mClover assay inserts the EGFP and mClover fluorescent protein into the LMNB and LMNA gene, respectively, using CRISPR-mediated DSBs and is therefore a direct measure of gene targeting (Pinder et al. 2015). Consistent with our screen results by siRNA depletion of PCAF, PCAF KO cells exhibited reduced HR repair in both gene targeting and HR cell-based assays, providing further support for a role for PCAF in DSB repair by HR (Fig. 3C; Supplemental Fig. S3E–G). The requirement for PCAF in HR-mediated processes was not limited to U2OS cells, as a reduction in gene-targeting efficiency was also observed in HeLa and HEK-293 cells upon PCAF depletion by siRNA (Supplemental Fig. S3H). Based on previous reports of PCAF also facilitating NHEJ (Ramachandran et al. 2016; Clouaire et al. 2018), we measured NHEJ by random plasmid integration assay (Miller et al. 2010). Consistent with other studies, we also observed a reduction in NHEJ in PCAF-deficient cells using this assay (Fig. 3C). These analyses suggest that PCAF promotes both main DSB repair pathways, HR and NHEJ.

To further analyze how PCAF participates in DNA repair, we monitored the recruitment of PCAF to DNA breaks using laser-microirradiation. Upon laser-induced DNA damage, GFP-tagged PCAF was recruited to DNA damage sites (Fig. 3D). PCAF contains three major functional domains: an N-terminal PCAF-specific domain, a central N-acetyltransferase (N-AT) domain, and a C-terminal bromodomain (Fig. 3E). To identify which domains mediate PCAF translocation to DNA damage sites, we generated a series of PCAF domain mutants: ΔN-terminal (ΔN-term; 1–320), ΔN-AT (503–651), and ΔC-terminal (ΔC-term; 740–832) (Fig. 3E). The ability of PCAF to concentrate at DNA damage sites was independent from the N-term and HAT domains but reliant on the BRD (Fig. 3F). These results were confirmed using chromatin fractionation following IR treatment, which showed that ectopically expressed SFB-tagged ΔC-term, which lacks the BRD, displayed reduced enrichment onto chromatin after IR compared to wild-type (WT) PCAF (Fig. 3G). Taken together, these data suggest that the BRD of PCAF is required for its DNA damage localization.

The BRD is a well-established reader domain that recognizes acetylated histones within chromatin (Chiang 2009; Filippakopoulos et al. 2012; Musselman et al. 2012). To identify which histone modification binds to the BRD of PCAF, we performed a modified histone peptide array with purified GST-tagged recombinant WT and ΔC-term PCAF proteins (Supplemental Fig. S3I). Full-length PCAF, but not PCAF lacking the BRD, bound to histone H4 peptides acetylated on residues K12, K16, and K20 (Fig. 3H). We next validated these interactions in PCAF expressing cells. Consistent with our in vitro data, WT full-length PCAF, but not PCAF lacking the BRD (i.e., ΔC-term), bound to acetylated H4 peptides (Fig. 3I). A key contributor to DNA damage-dependent acetylation of H4 is the HAT TIP60 (Ikura et al. 2000; Miller et al. 2010; Gong and Miller 2013; Tang et al. 2013; Gong et al. 2015). Indeed, TIP60 depletion impaired PCAF accrual at DNA damage sites (Fig. 3J; Supplemental Fig. S3J). Taken together, these results established PCAF as a DNA damage response factor that utilizes N-terminal acetylated H4 that is mediated by the HAT TIP60 to associate with DNA damage sites.
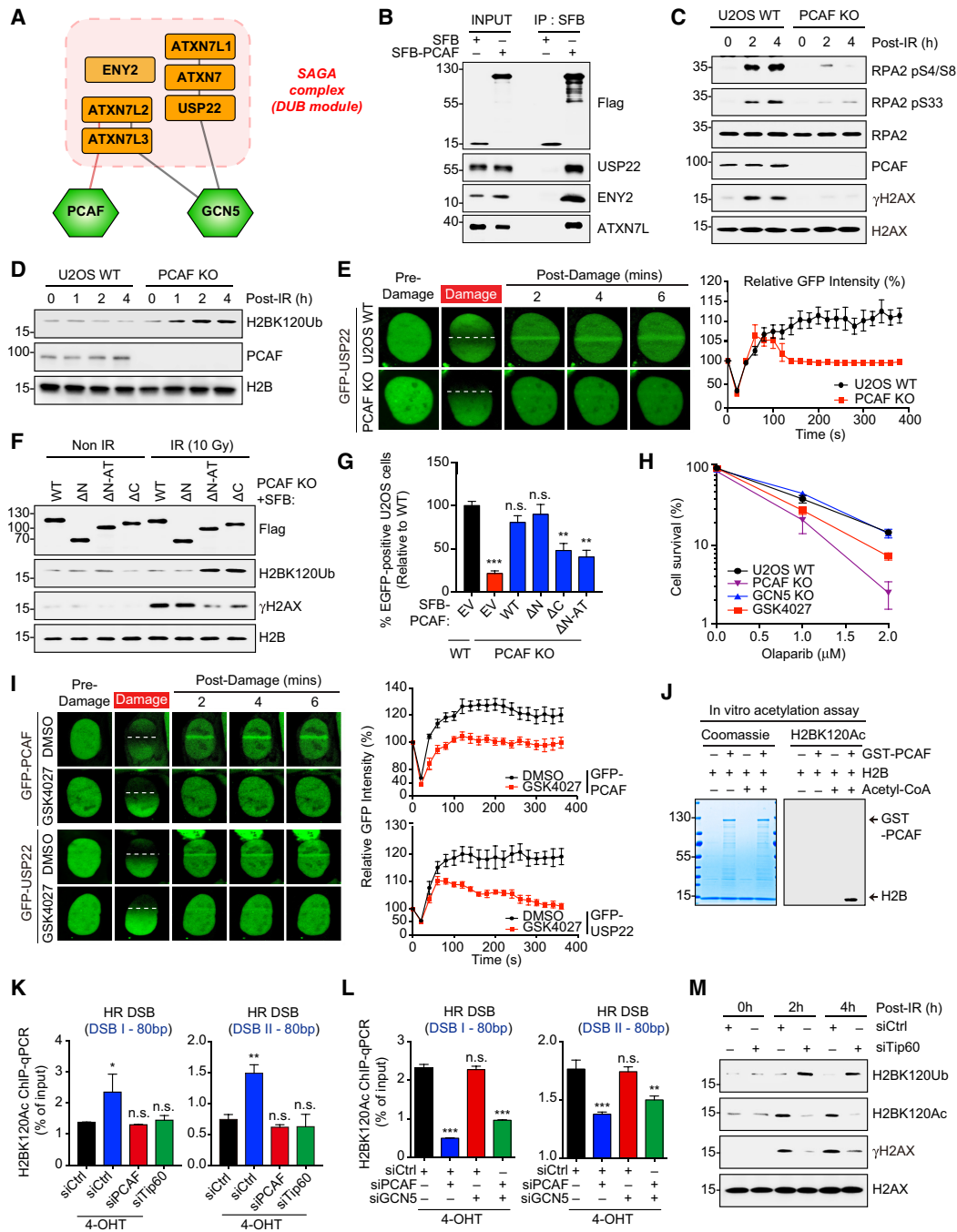
H2BK120 ubiquitylation-acetylation switch at DNA damage sites is mediated by PCAF and the SAGA complex

PCAF is a component of the SAGA complex, a large, multi-subunit transcriptional co-activator and histone modifying complex (Helmlinger and Tora 2017). In our AP-MS data, we identified many SAGA complex proteins as PCAF interactors (Figs. 2C, 4A). These interactors included SAGA factors specific for transcription binding, core structure, and DUB modules. A previous study reported that the SAGA deubiquitylating enzyme (DUB) module promoted DSB repair through H2B deubiquitylation, which facilitated ATM-mediated γH2AX foci formation, but the involvement of PCAF in DSB repair is unclear (Ramachandran et al. 2016). Streptavidin pull-down of SFB-tagged PCAF validated our AP-MS, as interactions between PCAF and the SAGA DUB components USP22, ENY2, and ATXN7L were observed (Fig. 4B). We next determined which domain was required for interactions between PCAF and the SAGA DUB module using WT and domain mutants of PCAF. We found that the ΔN-AT domain failed to bind components of the SAGA DUB module (Supplemental Fig. S3K). Together, these observations identified PCAF as an interactor of the SAGA DUB module and that this interaction requires the N-AT domain of PCAF.

To further define the role of PCAF in the DDR, we analyzed DNA damage signaling following IR treatment in
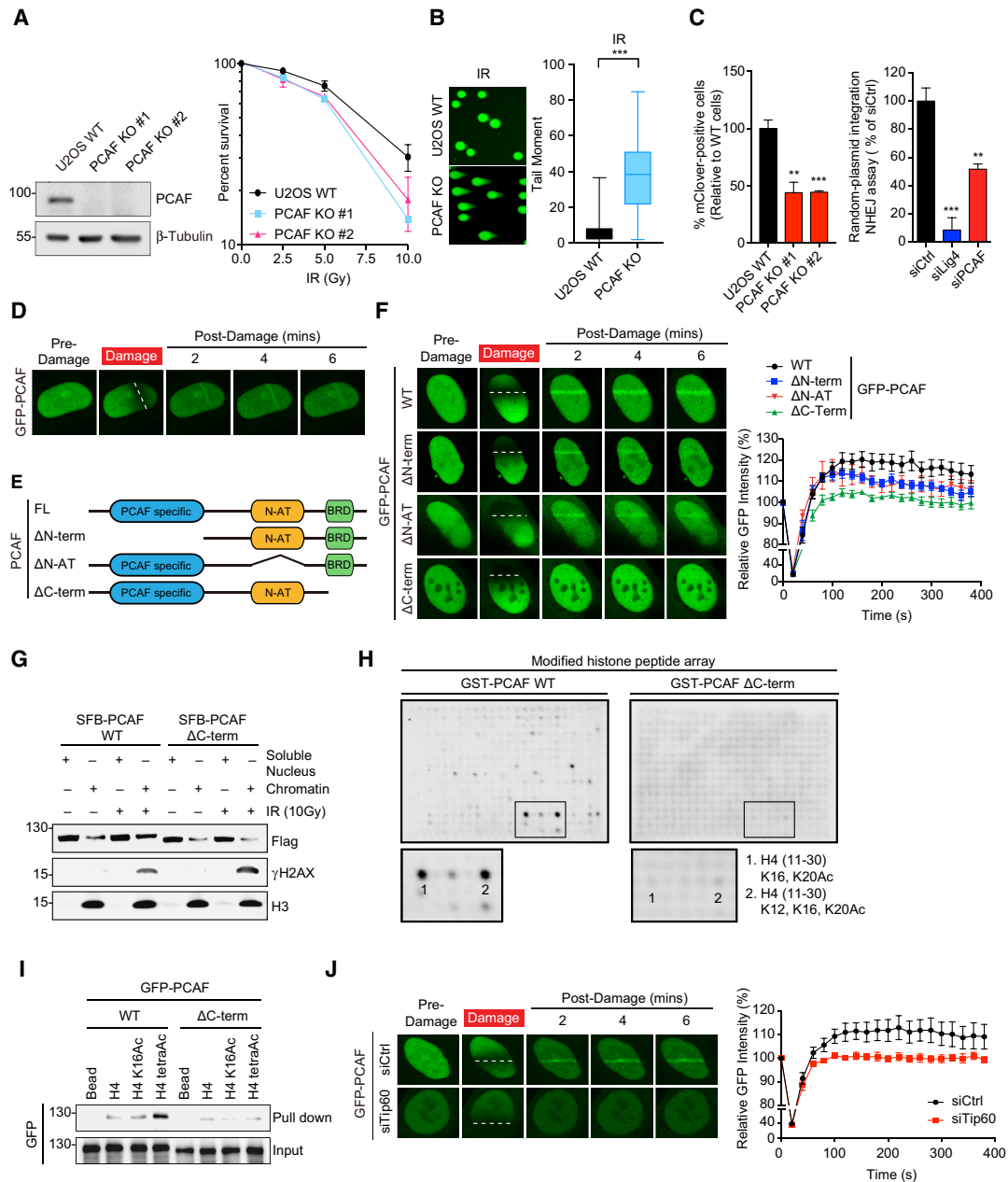
Figure 3. PCAF is a DNA damage response factor. (*A*) Knockout (KO) of PCAF by CRISPR/Cas9 in U2OS cells (*left* panel) and IR-sensitivity analyses by clonogenic assay (*right* panel). Knockout of PCAF was confirmed by western blotting with a PCAF-specific antibody. For IR sensitivity, colonies from undamaged and IR-damaged cells were counted, normalized to undamaged controls, and values were plotted as percent survival. Data represent the mean ± SEM; *N* = 3. (*B*) Loss of PCAF results in increased DSBs following ionizing radiation (IR) as detected by neutral comet assay (*left* panel, quantified in *right* panel). For all box-and-whisker plots, the box depicts 25%–75%, whiskers are 10%–90%, and the median is indicated. Data represent the mean ± SEM from >100 cells. (***) *P* < 0.001. (*C*) CRISPR-mClover HR assay (*left*) and random plasmid integration NHEJ assay (*right*). mClover-HR donor vector was transfected with Cas9-gRNA into U2OS WT or PCAF KO cells. Percentage of mClover-positive cells was normalized to control cells. NHEJ repair efficiency was analyzed by random plasmid integration assay with normalization to control cells. Data represent the mean ± SD; *N* = 3. (**) *P* < 0.01, (***) *P* < 0.001. (*D*) GFP-PCAF translocates to laser-induced DNA damage sites. (*E*) Schematic illustration of PCAF mutants. (*F*) C-terminal region (containing BRD domain) of PCAF promotes recruitment to DNA lesions. GFP-tagged PCAF mutants were monitored (*left* panel) and quantified (*right* panel) by live cell imaging using confocal microscopy. (*G*) C-terminal region (containing BRD domain) of PCAF is required for efficient chromatin binding. U2OS cells were fractionated following IR (10 Gy) treatment and analyzed by western blotting with indicated antibodies. (*H*) PCAF binds to acetylated histone 4 (H4Ac) via its C-terminal region (containing the BRD domain). A modified histone peptide array was performed with recombinant PCAF WT and C-terminal deletion mutant (*upper* panel). Lower black box shows a 2× magnification of original images with highly bound peptides indicated. (*I*) The C-term-containing BRD region of PCAF binds to H4ac. Biotinylated H4 peptides were incubated with GFP-PCAF WT and mutant overexpressed HEK-293 cell extracts and then immunoprecipitated with anti-GFP antibody. (*J*) Recruitment of PCAF to DNA lesions requires Tip60. GFP-tagged PCAF was monitored (*left* panel) and quantified (*right* panel) in siCtrl and siTip60 cells as in Figure 3F. For laser microirradiation experiments in *D, F,* and *J,* white dotted lines indicate laser paths and all images were normalized to undamaged regions. Data represent the mean ± SEM from >10 cells.

Figure 4. PCAF regulates H2BK120 ubiquitylation and acetylation to promote DSB repair. (*A*) PCAF protein interactome network, including the SAGA DUB module (see Fig. 2C). (*B*) PCAF interacts with the SAGA DUB module. Cell extracts from SFB-PCAF expressing HEK-293 cells were immunoprecipitated with streptavidin beads and analyzed by western blotting. (*C*) PCAF promotes DNA damage signaling following IR treatment. U2OS WT and PCAF KO cells were treated with IR, collected at the indicated times, and cell lysates analyzed by western blotting with the indicated antibodies. (*D*) H2BK120 ubiquitylation accumulates in PCAF KO cells after IR treatment. Samples were analyzed as in *C*. (*E*) PCAF promotes USP22 recruitment to DNA damage sites. GFP-tagged USP22 was monitored (*left* panel) and quantified (*right* panel) following laser microirradiation in U2OS WT and PCAF KO cell lines by confocal microscopy. White dotted lines indicate laser paths, and all images were normalized to undamaged regions. Data represent the mean ± SEM from >10 cells. (*F*) N-AT and C-terminal BRD domains promote H2BK120 deubiquitylation. PCAF KO cells were transfected with SFB-tagged PCAF WT and derivatives followed by western blot analysis as in *C*. (*G*) PCAF N-AT and C-terminal domains facilitate HR. HR was measured by Cas9/EGFP-LNMB1 HR assay. Data represent the mean ± SEM; $N = 3$. (**) $P < 0.01$, (***) $P < 0.001$, (n.s.) not significant. (*H*) Inhibition or depletion of PCAF sensitive to PARP inhibitor. Cells were treated with olaparib and GSK4027 as indicated. Cell survival was analyzed by clonogenic assays. Data represent the mean ± SEM; $N = 3$. (*I*) PCAF bromodomain inhibitor (GSK4027) suppresses PCAF and USP22 recruitment to DNA damage sites. GFP-tagged PCAF and USP22 were monitored (*left* panel) and quantified (*right* panel) following laser microirradiation in DMSO- and GSK4027-treated cells by confocal microscopy. White dotted lines indicate laser paths, and all images were normalized to undamaged regions. Data represent the mean ± SEM from >10 cells. (*J*) Recombinant PCAF acetylates H2BK120. An acetylation assay was performed with purified PCAF WT and H2B. H2BK120 acetylation was detected using a specific antibody. (*K,L*) PCAF but not GCN5 is required for H2BK120ac at DSBs. Site-specific DSBs in DIvA cells were analyzed by ChIP assays using the indicated primers. DSB I and II represent HR-prone DSB sites. Data represent the mean ± SEM; $N = 3$. (*) $P < 0.05$, (**) $P < 0.01$, (***) $P < 0.001$, (n.s.) not significant. (*M*) H2BK120 ubiquitylation to acetylation switch following DNA damage requires Tip60.

U2OS WT and PCAF KO cells. In PCAF knockout cells, γH2AX levels and downstream RPA phosphorylations were reduced compared with wild-type U2OS cells (Fig. 4C). We also observed a modest but reproducible decrease in H2BK120 ubiquitylation in control cells, consistent with a recent report identifying this histone mark as being removed at DSB sites (Clouaire et al. 2018). Interestingly, PCAF KO cells failed to reduce H2BK120ub levels following IR treatment and rather displayed increased H2BK120ub levels following DNA damage compared to control cells (Fig. 4D). PCAF and its associated DUB complex can deubiquitylate H2BK120 in vitro (Clouaire et al. 2018). Thus, PCAF and the SAGA DUB module may mediate the deubiquitylation of H2BK120 at DSBs (Clouaire et al. 2018). Given our observation that PCAF localizes to DNA damage sites and interacts with the SAGA DUB module, we analyzed DNA damage recruitment of the SAGA DUB components USP22 and ENY2 to DNA damage lesions by laser micro-irradiation. We observed rapid accumulation of USP22 and ENY2 at DNA damage sites, which were reliant on PCAF in ALT positive (U2OS) and ALT negative (HeLa) cell lines (Fig. 4E; Supplemental Fig. S3L,M). Given that the PCAF-related HAT GCN5 also interacted with the SAGA complex (Fig. 4A), we generated GCN5 knockout cells which exhibited comparable USP22 recruitment to DNA damage sites as parental cells (Supplemental Fig. S3N,O). These data indicated that PCAF, but not GCN5, regulates SAGA DUB module translocation to DNA damage lesions within acetylated chromatin, as well as the deubiquitylation of H2BK120 following DNA damage.

Our data suggested that PCAF requires its BRD domain, as well as the HAT TIP60, to optimally associate with DNA damage sites, highlighting the importance of acetylation in regulating PCAF DDR functions. To test the relationship between specific domains within PCAF and H2Bub, PCAF KO cells were reconstituted with WT PCAF and several derivatives (Fig. 3E), and H2Bub levels were monitored by western blotting. Expression of PCAF BRD and HAT domain mutants in PCAF KO cells did not rescue H2Bub and γH2AX levels after IR treatment compared to WT or N-terminal deletion PCAF (Fig. 4F). The BRD and HAT domains were also required for homologous recombination as measured in reconstituted PCAF KO cells subjected to cell-based HR assays (Fig. 4G). PCAF KO cells also exhibited sensitivity to the PARP inhibitor Olaparib, a phenotype associated with HR deficiency (Fig. 4H). Unlike cells that lack PCAF, GCN5 KO cells were similarly resistant to the PARP inhibitor as parental U2OS cells (Fig. 4H). Interestingly, the PCAF/GCN5 BRD inhibitor, GSK4027 (Humphreys et al. 2017), rendered cells sensitive to PARP inhibitors (Fig. 4H), which is consistent with the PCAF promoting HR through interactions including those mediated by the BRD domain (Fig. 4G). In addition to PARP inhibitor sensitivity, GSK4027 treatment also reduced recruitment of PCAF and USP22 to DNA damage sites, again consistent with the BRD of PCAF being an essential domain linking PCAF to its DNA damage functions (Fig. 4I). We also observed reduced GCN5 accumulation in GSK4027-treated cells, which

may point to an as-yet-unidentified DDR function of the BRD of GCN5 (Supplemental Fig. S3P).

We observed that the HAT domain, which is important for acetyltransferase activity of PCAF, also promotes an interaction with USP22. In an attempt to separate the HAT activity from the DUB interaction domain to assess the contribution of both acetylation and deubiquitylation of PCAF and USP22, we generated an enzymatically dead PCAF by installing two mutations in the core HAT domain (PCAF-YFAA [Y616A/F617A] mutant) (Supplemental Fig. S4A,B; Clements et al. 1999). While PCAF-YFAA interacted similarly to USP22 compared to WT PCAF, this mutant was unable to promote HR repair as efficiently as WT PCAF as determined using a gene-targeting assay (Supplemental Fig. S4C,D), These data demonstrate that the acetylation activity of PCAF is required for HR. We observed similar results using the PCAF HAT inhibitor garcinol (Balasubramanyam et al. 2004), which blocked H2BK120 acetylation in vitro (Supplemental Fig. S4E) while not affecting PCAF-USP22 interactions or recruitment of USP22 to DNA damage sites in treated cells (Supplemental Fig. S4F,G). We further generated deletion mutants of the HAT domain of PCAF and found that the central HAT domain of PCAF mediates its interaction with USP22 (Supplemental Fig. S4H). The crystal structure of the HAT domain has identified vital acetyl-CoA interactions that span this region, making a separation of function mutant of the HAT and USP22 interaction challenging (Clements et al. 1999). Regardless, our data have identified and mapped interactions between PCAF and USP22, as well as further revealing the importance of the HAT and BRD domains of PCAF in mediating DNA damage signaling and repair of DSBs by HR.

The observation of a H2BK120 ubiquitin to acetyl switch at DSBs (Clouaire et al. 2018) and the potential involvement of PCAF in mediating these events prompted us to test directly the involvement of PCAF in regulating H2BK120 acetylation. Recombinant PCAF acetylated H2B on lysine 120 (Fig. 4J), consistent with the finding that purified human SAGA complex from cells acetylates this site on H2B (Clouaire et al. 2018). To analyze the involvement of PCAF directly on H2B acetylation at DSBs, we analyzed H2B acetylation levels at DNA damage sites using the DIvA (DSB inducible via asiSI) cell line, which allows for site-specific generation of DSBs at both HR and non-HR prone sites, as well as analysis of histone PTMs, including acetylation at these DSBs (Miller et al. 2010; Aymard et al. 2014). Using ChIP analysis with anti-H2BK120ac antibodies followed by qPCR, we analyzed this mark in undamaged and damaged conditions (i.e., +4-OHT) at two HR-prone DSBs and two non-HR prone DSB sites. Upon DNA damage induction, we observed an increase of H2BK120ac at HR-prone DSBs (Fig. 4K), which is in line with a recent report identifying the induction of this histone mark at DSBs (Clouaire et al. 2018). Importantly, the acetylation of H2B on lysine 120 was dependent on both PCAF and TIP60 but not GCN5 (Fig. 4K,L; Supplemental Fig. S3Q). Finally, depletion of TIP60 mimicked the loss of PCAF, as these cells were unable to switch H2BK120 ubiquitylation to acetylation

following IR to regulate γH2AX levels (Fig. 4M). These experiments revealed a clear inverse relationship between H2Bub and γH2AX-H2Bac levels. As IR treatment was found to increase H2Bac levels with a concomitant increase in γH2AX, either TIP60 or PCAF deficiency inhibited these marks and resulted in an increase in H2Bub following DNA damage (Fig. 4F–M).

Our comprehensive genetic, cellular, and biochemical data revealed a new chromatin-mediated DSB repair pathway involving a TIP60-PCAF-SAGA DUB complex. Our data suggests that DSB-activated TIP60 mediates H4 acetylations that are bound by the BRD domain of PCAF that promote the retention of PCAF to chromatin at DSBs. PCAF then triggers a ubiquitin to acetylation switch on histone H2B lysine 120 via interactions with and the recruitment of the SAGA DUB module to damage sites. Following the deubiquitylation of H2B, PCAF then directly acetylates the unmodified lysine 120 of H2B, a requisite histone mark at DSBs that is required to promote HR repair. These data suggest that the repriming of chromatin from a transcription to repair-proficient state requires H2BK120ub conversion to H2BK120ac, which requires the TIP60-PCAF-SAGA DUB module repair axis.

### Endogenous DNA damage triggered by BET-BRD protein deficiencies requires transcription

Our screen for BRD proteins involved in DSB repair and the suppression of endogenous DNA damage identified several BET BRD proteins. Given the importance of BET BRD proteins in cancer and as therapeutic targets, we chose to study these proteins and their participation in genome integrity pathways in more detail. BET BRD protein inhibition by JQ1, which is an inhibitor of BET-proteins, resulted in increased γH2AX signaling and DSB formation (Fig. 5A–C). Similar results were observed in nontransformed, immortalized cells (Supplemental Fig. S5A). As JQ1 binds and inhibits all BET BRD family members, we individually depleted BRDT, BRD2, BRD3, and BRD4 to identify the targets of JQ1 whose inhibition resulted in increased endogenous DNA damage. Specific depletion of BRD2 and BRD4 significantly increased DSBs and γH2AX levels, suggesting that cells deficient in these BET BRD proteins were susceptible to spontaneous DSB formation (Fig. 5C; Supplemental Fig. S5B,C).

BET BRD proteins have been linked to DNA damage signaling and repair previously (Floyd et al. 2013; Li et al. 2018; Sun et al. 2018), although how these proteins function mechanistically to suppress DNA damage has remained elusive. Given our identification of increased endogenous γH2AX levels and micronuclei formation in BRD2- or BRD4-deficient cells (Fig. 1D–E), as well as the well-documented role of BET BRD proteins in transcriptional regulation (Yang et al. 2005; Wu and Chiang 2007; Bennardo et al. 2008; Devaiah et al. 2012; Patel et al. 2013; Di Micco et al. 2014; Baranello et al. 2016; Bhagwat et al. 2016), we hypothesized that altered transcriptional processes in BET BRD-deficient cells may generate intrinsic DNA damage. As a means to address our hypothesis, we cotreated cells with JQ1 and the transcriptional initia-

tion inhibitor triptolide (Bensaude 2011) and analyzed γH2AX levels, a surrogate marker for endogenous DNA damage. The inhibition of transcription by triptolide treatment was confirmed by nascent 5-EU incorporation (Supplemental Fig. S5D). Remarkably, inhibition of transcription suppressed endogenous DNA damage formation in JQ1-treated cells (Fig. 5D). Importantly, we observed the same effects in BRD2- or BRD4-depleted cells, which validated that these effects were due to specific inhibition of these BET proteins and not other targets of JQ1 (Supplemental Fig. S5E). These results demonstrated that BET inhibition-induced DNA damage is caused by a transcription-dependent process.

R-loops initiate DNA damage formation in BET-deficient cells

During transcription, the inability to release the nascent RNA transcript from the DNA template strand can result in RNA-DNA hybrids, also known as R-loops, which can trigger DSBs and genomic instability (Huertas and Aguilera 2003; Sollier and Cimprich 2015; Gaillard and Aguilera 2016; Marnef et al. 2017; Makharashvili et al. 2018; Puget et al. 2019). Given the connection between transcription and DNA damage that we observed upon BET BRD protein inhibition, we sought to test if altered R-loop formation/processing may be occurring in these cells, which could help explain the observed DNA damage and genome instability that occurs in BRD2- and/or BRD4-deficient cells (Figs. 1C,D, 5A–D). Using the well-documented S9.6 antibody that recognizes RNA-DNA hybrids (Boguslawski et al. 1986; Hu et al. 2006), we measured the accumulation of R-loops using immunofluorescence and cell imaging in control and JQ1-treated cells. While we observed robust cytoplasmic staining, likely a reflection of mitochondrial-associated R-loops (Pohjoismäki et al. 2010), we observed nuclear signals corresponding to nucleoli in control cells (Supplemental Fig. S5F). Interestingly, we observed an increase in the nuclear R-loop signal, both in nucleoli and nonnucleoli regions as detected with the nucleoli marker protein nucleolin, in JQ1-treated cells, which was also sensitive to RNaseH1 expression (Supplemental Fig. S5F). Importantly, expression of mCherry-tagged RNaseH1, which resolves R-loops, removed this signal, validating these results as detecting bona fide R-loops (Fig. 5E). To measure the accumulation of R-loops at specific DNA loci, we performed DRIP qRT-PCR in control and JQ1-treated cells, analyzing sites previously reported to be prone to R-loop formation. For example, the 5′ ETS regions and HIF1 α gene have been reported to accumulate R-loops in topoisomerase I-depleted cells (Manzo et al. 2018), and G-rich "pause" sequences of the β-actin gene are also prone to accumulate R-loops (Skourti-Stathaki et al. 2014; Hatchi et al. 2015). We observed that RNA-DNA hybrids were increased almost twofold in JQ1-treated cells and these signals were removed by RNaseH1 treatment (Supplemental Fig. S5G). We further validated these results using a different RNA-DNA hybrid pulldown method called R-ChIP. This method employs the pulldown of R-loops using an
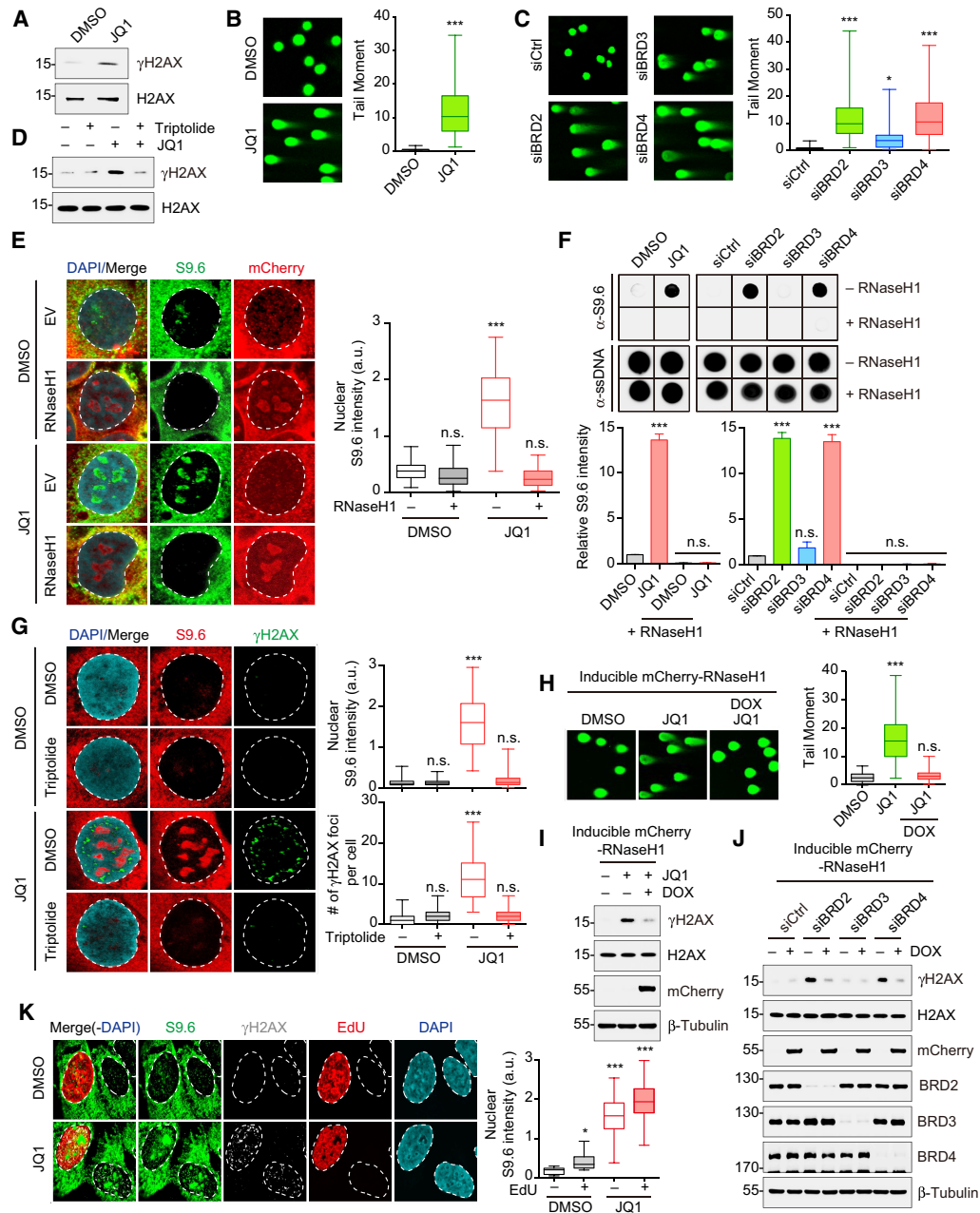
Figure 5. RNA-DNA hybrid-induced DNA breaks form in BET-protein inhibited cells. (*A–C*) Inhibition of BET proteins trigger DNA breaks. Cells treated with the BET-BRD protein inhibitor (JQ1) were analyzed by western blotting with the DNA damage marker γH2AX. (*B,C*) Cells were treated with JQ1 (*B*) or indicated siRNAs (*C*); DNA breaks were detected by neutral comet assay (*left* panel) and tail moments were quantified (*right* panel). Data represent the mean ± SEM from >100 cells. (*) $P < 0.05$, (***) $P < 0.001$. (*D*) Transcription promotes DSBs in BET protein-deficient cells. JQ1 and/or transcription inhibitor (triptolide) were added to U2OS cells and γH2AX was analyzed by western blotting. (*E*) Inhibition of BET-proteins induced R-loops. Immunofluorescence (IF) analysis was performed with S9.6 antibody and mCherry-tagged RNaseH1. Nuclear S9.6 intensities were quantified with Image J (*right* panel). Diminution of nuclear S9.6 signal by mCherry-tagged RNaseH1 overexpression confirmed R-loops. (*F*) Quantification of R-loops by dot blot. Cells were treated with JQ1 or indicated siRNAs and purified genomic DNA ± RNaseH1 was analyzed with S9.6 antibody and α-ssDNA as a loading control (*upper* panel). The intensity of S9.6 was measured by Image J and normalized to DMSO or siCtrl (*lower* panel). Data = mean ± SEM; $N = 3$. (*G*) R-loops, and their associated DNA damage, that form in BET-protein inhibited cells require transcription. R-loop and γH2AX accumulation was monitored by IF in the presence or absence of triptolide, and images were analyzed as in *E*. (*H*) BET-inhibition induced R-loop generated DSBs in BET-inhibited cells. Inducible mCherry-RNaseH1 cell lines were treated with JQ1 with and without doxycycline (DOX) and compared to DMSO control cells. DSBs were detected by neutral comet assay (*left* panel, quantified in *right* panel). Data represent the mean ± SEM from >100 cells. (*I,J*) Resolution of R-loops by RNaseH1 suppresses DNA damage in BET-inhibited cells. DNA damage was monitored as in *A* in the presence or absence of RNaseH1 in JQ1 (*I*) or BET-BRD protein siRNA-treated cells (*J*). (*K*) BET inhibition-mediated R-loops occur in replicating (EDU+) and nonreplicating (EDU-) cells. R-loops were analyzed as in *E*. Representative images are shown (quantified in *right* panel). For the IF experiments in *E–K*, data represent the mean ± SEM from >100 cells. For all box-and-whisker plots, the box depicts 25%–75%, whiskers are 10%–90%, and median is indicated. (*) $P < 0.05$, (***) $P < 0.001$, (n.s.) not significant.

mCherry-tagged catalytic mutant RNaseH1, which can bind but not resolve RNA-DNA hybrids (Chen et al. 2017), Consistent with the S9.6 DRIP assay, we observed increased mutant RNaseH1 binding to these sites in JQ1-treated cells, further demonstrating the presence of R-loops in BET-protein inhibited (Supplemental Fig. S5H).

To identify which specific BET BRD protein is responsible for suppressing R-loops, as JQ1 inhibits all BET BRD proteins, we depleted individual BET BRD proteins and performed S9.6 immunofluorescence to detect R-loops. While control and siBRD3 cells exhibited similar levels of R-loops, we observed that BRD2- and BRD4-depleted cells displayed increased R-loops, similar to JQ1-treated cells (Supplemental Fig. S6A). Again, expression of RNaseH1 removed the S9.6 signal, demonstrating the presence of increased R-loop structures in BRD2 and BRD4 siRNA-depleted cells (Supplemental Fig. S6A). These results are consistent with those obtained with the BET BRD protein inhibitor JQ1 and suggest that BRD2 and BRD4 are the specific factors that act to suppress excessive R-loop formation in cells (Fig. 5E; Supplemental Fig. S6A).

To further verify these results with multiple independent assays, we performed a dot blot analysis that allows detection and quantifications of R-loops from purified genomic DNA (see schematic in Supplemental Fig. S6B). R-loops were enriched in JQ1-treated, as well as BRD2- and BRD4-depleted, cells as measured by dot blot (Fig. 5F). These signals were sensitive to RNaseH1, confirming the detection of R-loops that formed in JQ1-treated or siRNA-depleted BRD2 or BRD4 cells. Using a fluorescently-tagged catalytic mutant RNaseH1 (mCherry-RNaseH1 mut) that is a robust sensor of R-loops in cells (Bhatia et al. 2014), we observed that R-loops levels increased at DNA damage sites in both JQ1-treated and BRD2/BRD4-depleted cells as measured by increased visualization of mCherry-RNaseH1 mut at laser microirradiated sites in these cells compared to control cells or undamaged regions of the cell (Supplemental Fig. S6C). Altogether, these data demonstrate that JQ1treatment increases R-loop formation in cells and that this is specific to the BET proteins BRD2 and BRD4, which are required to suppress excessive R-loop formation in cells.

To investigate whether R-loops were involved in generating DNA damage in BET protein-deficient cells, we analyzed DNA damage signaling and DSB formation in these cells with and without transcription or RNaseH1 overexpression. Consistent with our observation that transcriptional inhibition suppressed DNA damage induction in JQ1-treated or BRD2/BRD4-depleted cells (Fig. 5D; Supplemental Fig. S7A), we also observed a reduction in R-loop levels, as well as DNA damage when analyzed together in cells, upon transcription inhibition in both JQ1-treated and BRD2/BRD4-depleted cells (Fig. 5G; Supplemental Fig. S7A). In support of these data, recruitment of mCherry-RNaseH1 mut to laser-induced DNA damage-associated R-loops was dependent on transcription, which further validated our observation that increased R-loops in BET-deficient cells was reliant on transcription (Supplemental Fig. S7B). Remarkably, induced expression

of RNaseH1 reduced DNA damage signaling (i.e., γH2AX) and the formation of DNA breaks as detected by neutral comet assay in JQ1-treated and BRD2- or BRD4-depleted cells (Fig. 5H–J). Thus, these data identify transcription-generated R-loops as the source of DNA damage in cells deficient for the BRD proteins BRD2 or BRD4, as well as those treated with the small molecule BET BRD protein inhibitor JQ1.

Recently, induction of DSBs by R-loops has been shown to be associated with transcription-replication conflicts in human cells (Hamperl et al. 2017). To address if the DNA damage caused by R-loops associated with BET protein inhibition was formed in this manner, we investigated the cell cycle distribution of BET-inhibited cells to determine if there was a correlation between R-loops and DNA damage in replicating cells. Surprisingly, we observed R-loop formation and DNA damage induction by IF staining of S9.6 and γH2AX, respectively, in both replicating and nonreplicating JQ1-treated and BRD2- or BRD4-depleted cells (Fig. 5K; Supplemental Fig. S7C; note—EdU staining identifies replicating cells). Taken together, these data suggest that transcription-associated R-loops that trigger DNA damage in BRD2- and BRD4-deficient cells, as well as their cellular outcomes, do not occur solely by transcription-replication conflicts.

BRD2 regulates topoisomerase I activity to resolve R-loops

As a means to identify how inhibition of BET proteins stimulated R-loop formation, we analyzed BET protein interactions provided by our protein network analysis of BRD proteins (Fig. 2). Interestingly, these data captured an interaction between BRD2 and topoisomerase I (TOP1) (Fig. 6A). TOP1 acts to relax negative supercoils, activities known to reduce transcription-associated R-loop formation (Drolet et al. 1995; Massé et al. 1997; El Hage et al. 2010). To validate our protein network results, we performed immunoprecipitation with GFP-tagged BRD2 and observed that endogenous TOP1 bound to GFP-tagged BRD2 (Fig. 6B). To identify if these interactions were direct, we performed a far western blot analysis with recombinant proteins. Recombinant TOP1 protein directly interacted with BRD2, which implicated that this interaction may directly regulate TOP1 activity (Fig. 6C). To test this idea, we performed in vitro TOP1 activity assays with TOP1 alone and/or with recombinant BRD2 and other BET proteins. While addition of BET proteins alone did not affect the levels of supercoiled plasmid, TOP1 readily converted the supercoiled plasmid species to nicked and relaxed forms as expected (Fig. 6D). Interestingly, recombinant BRD2 stimulated TOP1 relaxation activity while BRD3 and BRD4 did not exhibit this behavior (Fig. 6D). BRD2 addition increased TOP1 activity in a dose-dependent manner, with quantification of supercoiled to relaxed forms exhibiting an almost threefold enhancement of TOP1 activity upon BRD2 addition compared to TOP1 alone (Fig. 6E). These results suggest that BRD2 protein deficiency, either by JQ1 treatment or by siRNA-mediated depletion, could decrease the
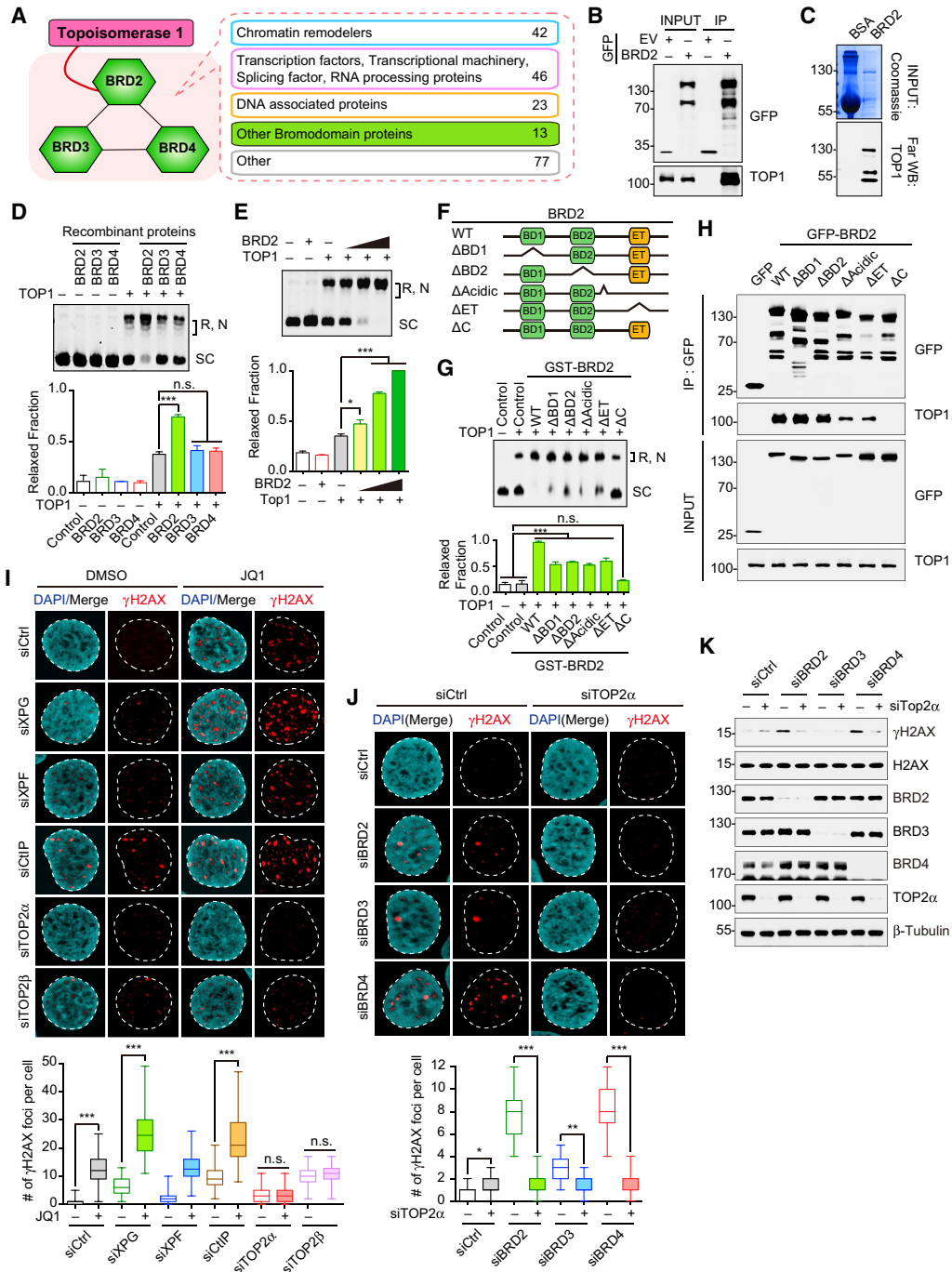
Figure 6. BRD2 regulates topoisomerase I to prevent topoisomerase II-dependent DNA damage. (*A*) Network analysis of BET proteins interactomes. BET-BRD proteins interact with topoisomerase I (TOP1). (*B*) BRD2 protein interacts with TOP1. GFP-tagged BRD2 was transfected into U2OS cells and immunoprecipitated with anti-GFP. Samples were analyzed by western blotting with indicated antibodies. (*C*) BRD2 directly interacts with TOP1 in vitro. A protein interaction assay was performed by far western using recombinant BRD2 and TOP1. (*D,E*) BRD2 promotes TOP1 relaxation activity. TOP1 activity was measured by a plasmid relaxation assay. Relaxed and nicked DNA was monitored by agarose gel electrophoresis. (SC) Super-coil DNA, (R,N) relaxed and nicked DNA. Data represent the mean ± SEM; $N = 3$. (*) $P < 0.05$, (***) $P < 0.001$, (n.s.) not significant. (*F*) Schematic illustration of BRD2 mutants. (*G*) BRD2 promotes TOP1 relaxation activity via its C-terminal domain. TOP1 activity was measured by plasmid relaxation assay as in *D,E*. (*H*) TOP1 interacts with the C-terminal domain of BRD2. Cell extracts from GFP-BRD2 WT and mutants expressing HEK-293 cells were immunoprecipitated with GFP antibody and analyzed by western blotting. (*I*) Topoisomerase II (TOP2)-induced DSBs after JQ1 treatment. γH2AX foci were monitored by immunofluorescence (*upper* panel) and quantification of γH2AX foci per cell was plotted (*lower* panel). Data represent the mean ± SEM from >100 cells. (***) $P < 0.001$, (n.s.) not significant. For all box-and-whisker plots, the box depicts 25%–75%, whiskers are 10%–90%, and median is indicated. (*J,K*) Cells were cotransfected with indicated siRNAs and siTOP2. DNA damage production was measured by immunofluorescence (*J*) and western blotting (*K*) using a γH2AX antibody. The number of γH2AX foci per cell was quantified, and data represent the mean ± SEM from >100 cells in *F*. (*) $P < 0.05$, (**) $P < 0.01$, (***) $P < 0.001$, (n.s.) not significant. For all box-and-whisker plots, the box depicts 25%–75%, whiskers are 10%–90%, and the median is indicated.

activity of TOP1, explaining the increased R-loop formation and subsequent endogenous DNA damage induction observed in these cells. An alternative explanation of these results could include TOP1 and BRD2 activities being involved in resolving R-loops once formed. As a means to address this possibility, we generated R-loops on in vitro plasmid templates as previously described (Stolz et al. 2019). As proposed by Stoltz et al., we also observed that the formation of R-loops in vitro generated a relaxed plasmid, which was not further topologically relaxed by the addition of TOP1 (Supplemental Fig. S7D). Taken together, these results suggest that TOP1 and its regulation by BRD2 act to inhibit R-loops from forming during transcription, but that once formed, these structures relax local topological stress, necessitating TOP1-independent activities for their resolution. To further understand how BRD2 regulates TOP1 activity, we identified a TOP1 binding region in the C terminus of BRD2 using a series of BRD2 truncation mutants, which was required to stimulate TOP1 activity in vitro (Fig. 6F,G). In line with these results, we observed a loss of BRD2-TOP1 interactions in cells, which was readily observed in WT BRD2 and several other BRD2 mutants but abolished in BRD2ΔC (Fig. 6H). To analyze the impact of disrupting BRD2-TOP1 interaction in cells, we depleted endogenous BRD2 and ectopically expressed WT and BRD2ΔC (Supplemental Fig. 8A). While expression of WT BRD2 rescued R-loop and DNA damage formation that was observed in siBRD2 cells, BRD2ΔC was unable to complement these cells (Supplemental Fig. 8B). Our data identify a BRD2-TOP1 interaction that is mediated by the C terminus of BRD2, which promotes the activity of TOP1 and is required to suppress DNA damage and R-loop generation that occurs in BRD2-deficient cells.

Although our results provided an explanation for how inhibition of BRD2 could trigger R-loop formation by reducing TOP1 activity, we also observed that the reduction of BRD4 resulted in R-loops and DNA damage. Interestingly, BRD4 was previously shown to regulate TOP1 activity by regulating RNAP II CTD phosphorylation (Baranello et al. 2016). The similar ability of BRD2 and BRD4 to regulate TOP I activity may explain why depletion of either of these BET BRD proteins, or treatment with the JQ1 inhibitor that targets both BRD2 and BRD4, result in increased R-loops and DNA damage. Regardless, our results have revealed that BRD2 and BRD4 functions during transcription are required to avoid unscheduled R-loop generation, which can trigger DNA damage formation.

Topoisomerase II activity promotes DNA damage in BET-deficient cells

Although our data identified BRD2 and BRD4 as suppressors of R-loops and their associated DNA damage in normal cells, the mechanisms governing DSB formation in BRD2- and BRD4-deficient cells remained unclear. Several pathways involved in R-loop-mediated DSBs have been identified. R-loop processing by XPG and XPF nucleases can generate DSBs (Sollier et al. 2014; Stork et al. 2016).

CtIP in association with TOP1-mediated single-stranded lesions can process R-loops into DSBs (Makharashvili et al. 2018). Topoisomerase II (TOP2)-generated DSBs can occur when RNAP II is paused (Ju et al. 2006; Haffner et al. 2010; Bunch et al. 2015). To test the potential involvement of these pathways, we monitored JQ1-induced γH2AX foci formation in cells individually depleted for several factors implicated in R-loop processing/formation. Depletion of XPG, XPF, or CtIP did not reduce γH2AX levels compared to control cells as measured by IF or western blot analysis in JQ1-treated cells (Fig. 6I; Supplemental Fig. S9A,B). These data were consistent with our determination that induction of DNA damage in JQ1-treated cells can occur in nonreplicating as well as replicating cells. However, we observed that depletion of TOP2α or TOP2β suppressed γH2AX levels in JQ1-treated cells (Fig. 6I; Supplemental Fig. S9C). As depletion of TOP2α suppressed DNA damage under these conditions, we further tested if depletion of TOP2α could alleviate DNA damage induction resulting from BET protein deficiency. Indeed, reduced TOP2α protein by siRNA-depletion or activity through the use of the TOP2 inhibitor dexrazoxane (which blocks TOP2 activity without generating DNA damage by trapped TOP2-DNA complexes [Classen et al. 2003]) reduced γH2AX levels in JQ1-treated and BRD2/BRD4-depleted cells (Fig. 6J,K; Supplemental Fig. S9D). The above results have identified TOP2 in promoting DNA damage following R-loop formation in BET BRD protein-deficient cells. These results are unlikely to be a mere consequence of suppressing R-loops upon TOP2α or TOP2β deficiency, as depletion of TOP2α or TOP2β resulted in increased formation of RNA/DNA hybrids that were induced upon BRD2 or BRD4 deficiency by siRNA-depletion or JQ1 treatment (Supplemental Fig. S9E,F). These data support topoisomerase II acting downstream of R-loops to trigger DNA damage that is generated upon BET BRD deficiency by JQ1 treatment or specific loss of BRD2 or BRD4.

It has been reported that aberrant TOP2 cleaved complexes require active transcription, as well as the proteasome and TDP2, to generate DNA breaks (Mao et al. 2001; Cortes Ledesma et al. 2009; Canela et al. 2019). Given the involvement of transcription in DNA breaks generated by BET BRD deficiency, we analyzed the potential use of the proteasome and TDP2, a tyrosyl-DNA phosphodiesterase enzyme that repairs TOP2-DNA lesions (Cortes Ledesma et al. 2009), in the processing of TOP2 into DNA breaks in JQ1-treated cells. We observed reduced DNA damage signaling and breaks in JQ1-treated cells when the proteasome was inhibited using MG132 (Supplemental Fig. S9G–I). We also detected a reduction in DNA damage signaling in TDP2-depleted cells compared to control cells upon JQ1 treatment (Supplemental Fig. S9J). These data suggest that the conversion of aberrant TOP2 cleaved complexes by etoposide or defective TOP2 that occurs upon BET BRD deficiency engage similar pathways to remove TOP2 to generate free DNA breaks that activate DNA damage signaling, including γH2AX (Supplemental Fig. S9; Canela et al. 2019).

Taken together, our data point to an important new relationship between BET BRD proteins and topological

stress pathways involving TOP1 and TOP2. Our data suggest that BET BRD proteins act to suppress aberrant R-loop formation during transcription through the coordinated regulation of topoisomerases that collectively keep R-loops in check to avoid the deleterious production of DNA damage, which can lead to genome instability and cell death.

Discussion

In this study, we have used a comprehensive approach to systematically identify human bromodomain proteins involved in DNA DSB repair and genome stability. Our data have revealed and established the BRD protein family as key modulators of DSB repair and, in particular, homologous recombination. Indeed, we have identified that out of the 40 ubiquitously expressed human BRD proteins, 24 promote HR repair. Generation of protein interaction networks of these BRD proteins has provided a rich resource of protein interactors and a framework by which to identify genome stability and DNA repair mechanisms involving BRD proteins (Fig. 7A). The discovery of over 47 newly identified BRD-BRD interactions increases the reported interactions between these chromatin reader proteins by nearly fourfold (Supplemental Fig. S10A). The potential of our study is demonstrated by the identification of two new genome integrity mechanisms involving the BRD proteins PCAF and BRD2/BRD4 reported here.

We show the HAT PCAF associates with DNA damage sites through its BRD in an acetylation-dependent mechanism to promote DSB repair. Although PCAF is an acetyltransferase enzyme, PCAF resides in a large transcription regulatory complex that contains the deubiquitylase enzyme (Nagy and Tora 2007), USP22, which has been shown to act on H2B during transcription (Zhao et al. 2008). A genome-wide analysis of histone modifications at DNA break sites identified a H2BK120 ubiquitin to acetylation switch at DNA damage sites (Clouaire et al. 2018). While previous work implicated PCAF in DSB repair (Ramachandran et al. 2016; Clouaire et al. 2018), our analysis has revealed that PCAF function in the DDR involves the DUB module of the SAGA complex and upstream acetylation signaling by the HAT TIP60. While we observed and confirmed interactions between PCAF and the SAGA DUB module, including USP22, deficiency in PCAF resulted in reduced USP22 accrual at DNA damage sites (Fig. 4). Both genetic and biochemical investigations of PCAF interactions with DNA damage sites and chromatin demonstrated that PCAF interacted with H4 acetylations in a BRD domain-dependent manner that required TIP60 to promote its localization to DNA damage sites. In support of the role of TIP60 in this pathway, loss of TIP60 reduced H2BK120ac at DNA lesions with a concomitant increase in H2BK120ub (Fig. 4K,M). We also determined that PCAF directly acetylates H2BK120 (Fig. 4J), suggesting a model whereby TIP60 acetylates H4 at DNA damage sites, which subsequently acts to recruit PCAF and its associated DUB, USP22, to DNA damage sites where they work together to

convert H2BK120ub to H2BK120ac to promote DSB repair (Fig. 7B).

While this work has defined a TIP60-PCAF-SAGA DUB module axis involved in modifying chromatin at break sites to promote repair, the precise role of H2BK120 ubiquitylation and acetylation in DNA repair remains unclear. H2BK120ub is involved in promoting the elongation of RNAP II during transcription (Xiao et al. 2005; Wu et al. 2014). DNA damage results in a reduction of elongating Pol II and subsequent transcriptional repression at transcription-associated DNA lesions (Shanbhag et al. 2010), which may involve PCAF. In support of this notion, TIP60 represses transcription following DNA damage (Gong et al. 2015), which may explain its involvement in regulating the DNA damage accumulation of PCAF and subsequent H2Bub to H2Bac switch at DNA damage sites. Our data do not rule out that H2Bub/ac may also alter chromatin structure at damage sites, as H2Bub blocks higher-order chromatin structure (Fierz et al. 2011), and compaction of chromatin has been observed at damage sites and proposed to be involved in HR repair (Khurana et al. 2014; Oberdoerffer 2015). We speculate that H2Bac may recruit a BRD protein to damage sites. Consistent with this idea, isolated BRD domains from SMARCA2, SMARCA4, SP140, and p300, have been shown to bind H2BK120ac (Filippakopoulos et al. 2012). Interestingly, several of these proteins were identified in our screens as being damage-associated and required for repair. Whether or not these BRD proteins recognize H2BK120ac at DNA damage sites to promote HR awaits future investigation.

It is well established that aberrant transcription can threaten genome integrity, including through the direct formation of DNA breaks and the production of R-loops (Marnef et al. 2017; Crossley et al. 2019). A potentially surprising finding from our data was the identification of the BET BRD proteins BRD2 and BRD4 as key mediators in suppressing transcription-associated R-loops and DNA damage. Inhibition of BRD4 was previously reported to induce DNA damage through a DNA damage signaling insulator function (Floyd et al. 2013); however, our data suggest that the source of endogenous DNA damage in BET BRD protein-inhibited cells is triggered by aberrant transcription. BRD4 associates with the positive transcription elongation factor b (P-TEFb) complex to promote transcription elongation (Jang et al. 2005; Yang et al. 2005) but also participates in regulating topoisomerase I (TOP1) to overcome the topological constraints of DNA supercoiling that occur during active transcription (Baranello et al. 2016). How then does BRD2 or BRD4 inhibition result in transcription and R-loop-dependent DNA breaks?

Based on our data, we propose that the activation of TOP1 and resolution of DNA topology by BRD4 and BRD2, as identified here, are critical functions of BET BRD proteins in maintaining genome stability through the suppression of R-loops that can generate DNA breaks. This idea is supported by our identification of increased R-loop formation and DNA damage in cells where BRD2 or BRD4 are either inhibited by JQ1 or depleted by siRNA. The suppression of DNA damage by RNaseH1 expression

Kim et al.
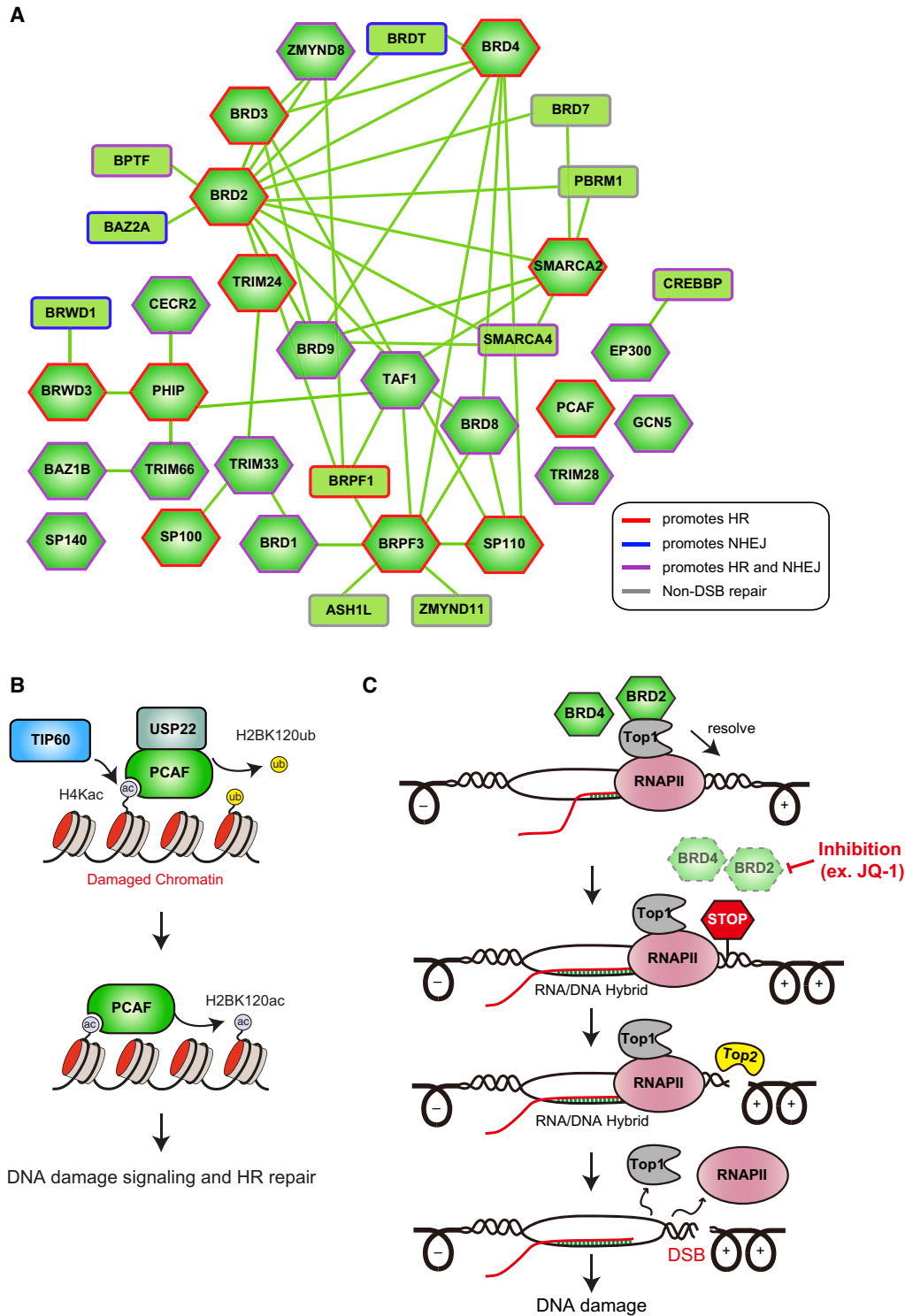
Figure 7. Systematic analysis of BRD proteins in human cells reveals roles in maintaining genome integrity. (*A*) Interaction network of human BRD proteins involved in DNA repair. Human BRD proteins display high levels of connectivity and widespread involvement with DSB repair, especially HR. BRD bait proteins are shown in green hexagons; other BRD proteins in green rectangles. (*B*) Model of PCAF in DSB repair. PCAF translocation to DNA damage sites is reliant on H4 acetylation by Tip60. PCAF recruits the DUB USP22 to deubiquitylate H2BK120 and directly acetylate H2BK120. PCAF thus regulates the H2BK120 PTM switch from ubiquitin to acetylation at DNA damage sites. (*C*) Model for BET-BRD protein promotion of transcription that suppresses R-loop formation and genome instability via regulation of TOP1 activity. BRD2 and BRD4 promote TOP1 activity to inhibit R-loop formation during transcription. Depletion or inhibition of BRD2 and BRD4 induces R-loop accumulation and TOP2-dependent generation of DSBs, which may resolve R-loop/RNA polymerase II obstructions.

or inhibition of transcription in these cells suggests that transcription-generated R-loops are the structures that are responsible for causing DNA damage in these settings. These results also support that R-loop suppression by BET BRD proteins BRD2 and BRD4 is direct, and is not an indirect consequence of gene expression changes that could occur upon their inhibition. Supporting a direct role for BET BRD proteins in R-loop suppression, we identified BRD2 as a direct interactor and stimulator of TOP1 activity, suggesting that an inability to fully activate TOP1 either directly by BRD2 or through RNAP II modification by BRD4 is likely to explain the increased R-loop formation and DSB generation that accompanies BRD2 or BRD4 inhibition. This notion is consistent with the known role of TOP1 in suppressing R-loops and genomic instability (Tuduri et al. 2009; El Hage et al. 2010; Li et al. 2015). RNAP II pausing can also increase R-loops (Zhang et al. 2017; Shivji et al. 2018), suggesting that reduced RNAP II elongation in BRD2/BRD4-deficient cells may also contribute to these phenotypes. However, perhaps counterintuitively, JQ1 treatment has been shown to result in increased RNA synthesis (Bowry et al. 2018), which may exacerbate the requirement for TOP1 activity in BET BRD-deficient settings due to aberrant transcription. We observe similar increases in nascent transcription in JQ1-treated or BRD4-depleted cells, while in BRD2 deficient cells, we observed a reduction in RNA synthesis (Supplemental Fig. S10B,C). These observations suggest a complex relationship between transcription and BET BRD proteins that must be tightly regulated to avoid DNA damage stress. Regardless, defects in transcription upon BET BRD inhibition, as well as our data identifying BRD2 as a stimulator of TOP1 activity, may help to explain the synergistic cell killing that is observed with the TOP1 poison camptothecin and JQ1 (Baranello et al. 2016). Our results suggest that R-loops and the pathways that govern their processing/regulation may participate in the therapeutic responses of BET inhibitors, an important question worth assessing further for these compounds that are actively being developed and used in therapeutic applications.

We observed that a consequence of increased R-loop formation in BET BRD-deficient cells was the production of DNA breaks. A number of endonuclease enzymes have been shown to act on R-loops, which can lead to DSBs, including XPG, XPF, CtIP, TOP1, and TOP2 (El Hage et al. 2010; Sollier et al. 2014; Makharashvili et al. 2018), reviewed in (Marnef et al. 2017; Crossley et al. 2019). Our genetic analysis of these factors in BET BRD-inhibited cells identified TOP2 specifically as the enzyme responsible for generating DSBs in these cells. R-loop-mediated DNA damage upon BET BRD inhibition occurred largely independently of the cell cycle, suggesting that these breaks are not merely a consequence of transcription-replication conflicts, which are known events that trigger DSBs as a result of R-loops (Hamperl et al. 2017; Crossley et al. 2019). In the absence of TOP1, TOP2 has been shown to resolve R-loops in the rDNA in yeast (El Hage et al. 2010). TOP2 is also involved in gene activation, where it has been shown to generate DSBs (Ju et al. 2006; Haffner

et al. 2010; Madabhushi et al. 2015), and these breaks have been proposed to be involved in RNAP II transcription elongation (Bunch et al. 2015). Importantly, TOP2-mediated breaks are observed in neuronal cells, which are not actively cycling, showing that TOP2 breaks can occur throughout the cell cycle (Madabhushi et al. 2015). We propose that the R-loops that accumulate in BRD2- and BRD4-deficient cells are targets for TOP2, whose activity results in heightened DSB formation (Fig. 7C). The decrease in TOP1 activity resulting from BRD2 or BRD4 inhibition may lead to TOP2-dependent breaks that act to resolve the transcriptional pausing and R-loops that accumulate in cells deficient for BRD2 or BRD4 activity.

There are several possibilities to explain why TOP2 generates breaks under these conditions. We and others have shown that BET BRD proteins are involved in DSB repair, which may result in unrepaired breaks when BRD2/4 are inhibited (Fig. 1B; Li et al. 2018; Sun et al. 2018). Mechanistically, the requirement for BRD2 and BRD4 in DSB repair by HR may stem from their involvement in R-loop regulation, which is implicated in DSB repair (for review, see Crossley et al. 2019), and/or by gene expression functions, as BRD4 has been shown to regulate the HR factor CtIP (Sun et al. 2018) and BRD2 may similarly regulate genes involved in HR. We can also not rule out that BET BRD proteins regulate TOP2 activity, given their involvement in regulating the topological resolving enzyme TOP1 during transcription (Fig. 6; Baranello et al. 2016). Regardless, the identification of R-loops and TOP2-dependent breaks in JQ1-treated cells may inform the potential interplay between these pathways in therapeutic targeting of BET BRD proteins. For example, JQ1-treated cells may be reliant on DSB repair given the increased breaks associated with BET BRD protein inhibition. This is in line with the recent findings that BET BRD inhibitors synergize with PARP inhibitors (Karakashev et al. 2017), which generate DNA breaks and impede DSB repair (Ray Chaudhuri and Nussenzweig 2017). Furthermore, potential genetic as well as therapeutic interactions between R-loop metabolism and BET BRD protein inhibitors should now be analyzed based on the R-loop suppressive function of BRD2 and BRD4 identified here.

Bromodomain proteins are key epigenetic factors that are best studied for their functions in regulating gene expression. Our systematic and deep interrogation of human BRD proteins has revealed a highly connective and indispensable family of proteins that govern genome integrity, including by promoting the repair of DSBs by homologous recombination and suppressing R-loops that generate DNA breaks. Indeed, we have determined that over half of BRD proteins participate in DNA double-strand break repair, and our generation of BRD protein interaction networks has illuminated a multitude of new protein-protein interactions, including those that enabled the identification of two new BRD-dependent genome maintenance mechanisms reported here. Future studies are warranted to analyze the potential involvement of other BRD proteins in R-loop regulation and other DNA transactions that can generate DNA damage, including replication.

Kim et al.

The propensity of BRD proteins to interact with each other and participate in transcription, as well as genome stability and DNA repair as determined here, point to important functional and physical interactions of BRD proteins that govern genome maintenance. Given the involvement of BRD proteins in human diseases, including cancer (Gong et al. 2016; Fujisawa and Filippakopoulos 2017), and their potential for therapeutic targeting (Barbieri et al. 2013; Stathis and Bertoni 2018), our comprehensive analysis of BRD proteins will likely assist ongoing efforts to convert mechanistic understanding of BRD proteins in diseases to therapeutic opportunities.

Materials and methods

Cell lines and cell culture

Human osteosarcoma (U2OS), human embryonic kidney (HEK-293), human cervical adenocarcinoma (HeLa), BJ-hTERT, and MRC5-hTERT cell lines were maintained in Dulbecco's modified Eagle's medium (DMEM) supplemented with 10% fetal bovine serum (FBS), 2 mM L-glutamine, 100 U/mL penicillin, and 100 μg/mL streptomycin. Inducible cell lines (HEK-293 for SFB-tagged proteins, U2OS cells for mCherry-tagged RNaseH1) were established and maintained in medium with 0.2 mg/mL hygromycin B.

siRNAs, primers, chemicals, and antibodies

siRNA and primer sequences, chemicals, and antibodies are summarized in Supplemental Tables S4–S7. All JQ1, triptolide, and dexrazoxane treatments were performed for 4 h with a final concentration of 500 nM, 1 μM, and 50 μM, respectively. Garcinol and GSK4027 treatments were performed for 24 h with a final concentration of 20 μM.

Cloning and plasmids

BRD genes were cloned into the pENTR Gateway vector as described previously (Gong et al. 2015), and the detailed information is summarized in Supplemental Table S3. The pENTR clones were transferred into GFP-, GST-, or SFB-tagged DEST vectors using the Gateway LR Cloning system (Invitrogen). Full-length PCAF was generated by PCR amplification from U2OS cDNA and cloned into the Gateway entry vector. PCAF and BRD2 mutants were constructed by PCR based on the full-length WT entry clone. All mutants were validated by DNA sequencing, and each primer set used in this study is described in Supplemental Table S5.

Generation of inducible cell lines and knockout (KO) cell lines

To establish the inducible SFB-tagged BRD protein-expressing cell lines, pcDNA5/FRT/TO containing SFB-tagged constructs were transfected with pOG44 Flp Recombinase expression vector into Flp-In T-REx HEK-293 cells. After 48 h, cells were treated with 0.2 mg/mL hygromycin B (Invitrogen) for selection of transfected cells. The inducible RNase H1 (WT or mutant)-expressing cell lines were generated using the same strategy as BRD proteins. pcDNA/FRT/TO containing the mCherry-tagged RNase H1 construct was transfected with pOG44 into Flp-In T-REx U2OS cells. PCAF and GCN5 knockout (KO) cell lines were generated by the CRISPR/Cas9 system. Individual gRNAs (PCAF and GCN5 gRNAs) were subcloned into pSpCas9 (BB)-2A-Puro (PX459,

Addgene #48139) and then stably transfected into U2OS cells using Lipofectamine 2000 (Invitrogen). Transfected cells were selected by 500 ng/mL puromycin for 3 d. Single cells were isolated by limited dilution using 96-well plates, and the levels of endogenous protein were analyzed by western blotting with the indicated antibodies (PCAF, Cell Signaling, #3378; GCN5, Cell Signaling, #3305). The gRNA sequences used in this study are described in Supplemental Table S5.

HR and NHEJ repair assay

U2OS-based HR and NHEJ reporter cells were transfected with the indicated siRNAs by Lipofectamine RNAiMax (Invitrogen). On the following day, the I-SceI-expressing vector (pCAG-I-SceI) was transfected into HR and NHEJ reporter cells, respectively. Forty-eight hours after I-SceI transfection, cells were harvested and washed with PBS and then resuspended in sodium citrate solution without fixation. The percentages of GFP-positive cells were analyzed by an Accuri Flow Cytometer (Fong et al. 2015). For the CRISPR-mClover HR assay (Arnoult et al. 2017), the mClover-HR donor plasmid and Cas9-gRNA vector were transfected into indicated cells. The Cas9-LMNB HR assay was transfected with the EGFP-LMNB HR donor and Cas9-gRNA vector (Roberts et al. 2017). After transfection, cells were incubated for 72 h and analyzed by an Accuri Flow Cytometer (BD Biosciences) (Fong et al. 2015) to detect the percentages of GFP-positive cells. A random plasmid integration assay was performed as previously described (Miller et al. 2010). Briefly, U2OS WT and PCAF KO cells were transfected with indicated siRNAs and the linearized pEGFP-C1 plasmid (BamHI and XhoI). On the following day, transfected cells were plated into two duplicate plates. One plate was incubated with 0.5 μg/mL G418 to detect NHEJ efficiency and the other plate incubated with normal media to calculate plating efficiency. Cells were grown for 2 wk, and colonies were stained using clonogenic assay methods. NHEJ efficiency was normalized to an siControl.

Immunofluorescence

After indicated treatments, cells were pre-extracted with CSK buffer (10 mM PIPES, pH 6.8, 100 mM NaCl, 300 mM sucrose, 3 mM MgCl$_2$, 1 mM EGTA, 0.5% [v/v] Triton X-100) on ice for 5 min and were fixed with 2% paraformaldehyde (PFA) at room temperature for 15 min. After washing with PBS, cells were blocked with 3% BSA in TBST for 30 min and incubated with the indicated primary antibodies at 4°C for 18 h. Cells were then washed 3× in PBS and stained with the appropriate secondary antibody at room temperature for 1 h. Cover slips were mounted onto 1.2-mm glass slides using Vectashield mounting medium containing DAPI (Vector Labs) and analyzed by FV10-ASW3.1 software on a Fluoview 3000 confocal microscope (Olympus).

Clonogenic cell survival assay

Clonogenic cell viability was examined using a colony-forming assay. Briefly, U2OS cells were transfected with the indicated siRNAs, and 24 h later, cells were seeded into 6-cm plates. Cells were treated with ionizing radiation (0–8 Gy) or Olaparib (0–2 μM) on the following day and incubated for 14 d in a tissue culture incubator (37°C, 5% CO$_2$). Colonies were fixed with methanol and stained with crystal violet solution (0.5% crystal violet in 20% ethanol). Results were normalized to plating efficiencies of untreated cells for each siRNA.

Tandem affinity purification (TAP)

Tandem affinity purification was performed as previously described with minor modifications (Leung et al. 2017). Briefly, inducible SFB-tagged BRD proteins expressed in HEK-293 cells were treated with tetracycline (1 µg/mL) for 24 h. Cells were lysed with NETN buffer (150 mM NaCl, 1 mM EDTA, 10 mM Tris-HCl, pH 8.0, and 0.5% [v/v] NP-40) supplemented with TurboNuclease (Accelagen) and 1 mM $MgCl_2$ at 4°C for 1 h. The supernatants were collected by centrifugation and incubated with 300 µL of streptavidin beads (GE Healthcare) overnight at 4°C. The beads were washed with NETN buffer, and bound proteins were eluted two times with 1 mL of biotin solution (2 mg/mL biotin in NETN buffer). The eluted samples were incubated for 4 h with 40 µL of S-protein beads (Novagen) at 4°C. The beads were washed three times with NETN buffer. The samples were eluted by boiling with 2× Laemmli buffer and resolved by SDS-PAGE for mass spectrometry analysis. The detailed procedures of our mass spectrometry (MS) analyses are described in Supplemental Materials and Methods. All AP-MS proteomic data have been deposited in the public data repository; PRoteomics IDEntifications (PRIDE) database.

Live cell imaging

Laser-induced DNA damage was generated using a Fluoview 3000 confocal microscope (Olympus), and recruitment levels of proteins were quantified by FV-10-ASW3.1 software. In brief, cells were seeded onto glass-bottom dishes (Ted Pella) and were presensitized by adding 10 µM BrdU for 20 h before laser-induced damage. Laser damage was induced using a 405-nm laser beam (60%) in a temperature-controlled chamber (37°C, 5% CO_2), and all images were captured using a 60× oil objective lens. The fluorescence intensity at the damage sites was analyzed using FV10-ASW3.1 software and normalized with the intensity of a nondamaged region.

Chromatin fractionation

Chromatin fractionation was performed as previously described (Wysocka et al. 2001). Briefly, 1×10^7 cells were harvested and washed with PBS. Cells were lysed in 200 µL of buffer A (10 mM HEPES, pH 7.9, 10 mM KCl, 1.5 mM $MgCl_2$, 0.34 M sucrose, 10% glycerol, 1 mM dithiothreitol, and protease inhibitor). Triton X-100 (final concentration 0.1%) was added to the lysate, which was incubated on ice for 8 min. Nuclei were collected by centrifugation at 1300g for 5 min at 4°C, and the pellet was washed with 500 µL of buffer A. Washed nuclei in the pellet were lysed in 100 µL of buffer B (3 mM EDTA, 0.2 mM EGTA, 1 mM dithiothreitol, and protease inhibitor) for 30 min on ice and centrifuged at 1700g for 5 min at 4°C. The supernatant contained the soluble nuclear fractions and the pellet was the insoluble chromatin fractions. The chromatin fraction was washed once with 500 µL of buffer B and resuspended in 200 µL of 2× SDS-Laemmli buffer. Samples were boiled for 10 min before analyzing by western blotting.

Histone modification binding assay and peptide pull-down assay

These experiments were performed as previously described (Gong et al. 2015). For the histone modification binding assay, a modified histone peptide array (Active Motif) was blocked with 5% (v/v) nonfat milk in TNT buffer (50 mM Tris-HCl, pH 7.5, 150 mM NaCl, 0.05% [v/v] Tween-20) and then incubated with the indicated recombinant proteins at 4°C for 1 h. The histone pep-

tide array was washed three times with TNT buffer and detected with HRP conjugated antibody. To validate the results of the histone peptide array, peptide pulldown assays were carried out using PCAF-expressing cell extracts. Biotinylated H4 peptides were incubated with PCAF-expressing HEK-293 cell extracts at 4°C for 1 h. Samples were pulled down with streptavidin Dynabeads (Invitrogen), and bound proteins were detected by western blotting using the indicated antibodies.

Neutral comet assay

DNA double-strand breaks were monitored using a CometAssay Reagent Kit (Trevigen) according to the manufacturer's instructions. In brief, U2OS cells were transfected with indicated siRNAs or plasmids. After 48 h, each cell was treated with the indicated reagents and then harvested. The cells were mixed with LMAgarose (Trevigen) and placed on a glass slide. Cells were lysed with 100 µL of lysis solution (Trevigen) for 1 h at 4°C and electrophoresed (1 V/cm^2) for 40 min in TBE buffer. Samples were fixed with 70% ethanol for 10 min and dried overnight. The DNA was stained with SYBR-green (Invitrogen), analyzed by fluorescence microscopy, and comet tail moments were calculated by counting 100 cells for each sample and analyzed with Image J (v 1.48). Tail moment (TM) reflects both the tail length (TL) and the fraction of DNA in the comet tail (TM = % DNA in tail × TL/100).

Immunoprecipitation

Cells expressing SFB-, or GFP-tagged proteins were lysed in NETN buffer (10 mM Tris-HCl, pH 8.0, 150 mM NaCl, 0.5% (v/v) NP-40, protease inhibitor cocktail) containing TurboNuclease (Accelagen) at 4°C for 1 h. Cell lysates were centrifuged at 15,000 rpm at 4°C for 10 min. SFB- or GFP-tagged proteins were immunoprecipitated with streptavidin Dynabeads (Invitrogen) or GFP-Trap beads (ChromoTek) at 4°C for 6 h. Next, beads were washed with NETN buffer, and bead-bound proteins were eluted with SDS sample buffer. Boiled supernatants were separated by 8%–16% SDS-PAGE, and proteins were detected by immunoblot with the appropriate antibodies.

Chromatin immunoprecipitation (ChIP) assay

ChIP assays were performed as previously described (Shanbhag et al. 2010; Aymard et al. 2014). Briefly, cells were crosslinked for 10 min with 1% PFA and then quenched with glycine. Next, cells were lysed with SDS buffer and sonicated. The samples were centrifuged, and the supernatants were incubated with primary antibodies at 4°C for 18 h. Antibody-bound protein/DNA complexes were pulled down using Protein G Dynabeads (Invitrogen) and eluted with elution buffer. Eluted protein/DNA complexes were digested with protease K, and purified DNA was analyzed by qRT-PCR for HR prone (HR DSB) or non-HR prone (Non-HR DSB) sites. All primer sequences used are described in Supplemental Table S5. The R-loop ChIP assay is described in Supplemental Materials and Methods.

Immunofluorescence for RNA-DNA hybrid analysis

U2OS cells were treated with the indicated inhibitor or transfected with the indicated siRNAs. After incubation, each cell was washed with 2% paraformaldehyde at room temperature and fixed with 100% ice-cold methanol at 4°C for 5 min. Next, cells were blocked with 3% BSA/TBST at room temperature for 1 h

Kim et al.

and incubated with S9.6 (Kerafast, #ENH001) and γH2AX antibody (Novus Biologicals, #NB100-384) at 4°C for 18 h. Cells were washed three times with PBS and then incubated with appropriate secondary antibody in 3% BSA/TBST at room temperature for 1 h. After washing, each cover slip was mounted onto 1.2-mm glass slides using Vectashield mounting medium containing DAPI (Vector Labs). RNA-DNA hybrids were detected by a Fluoview 3000 confocal microscope (Olympus), and nuclear S9.6 signals were quantified using Image J (v 1.48). The cytoplasmic and nucleolar S9.6 signals were excluded by overlaying DAPI-less regions, which correspond to nucleoli. Results were confirmed with nucleolin staining by IF.

In vitro topoisomerase I (TOP1) activity assay

In vitro topoisomerase I activity was analyzed using the Topoisomerase I Assay kit (Topogen) following the manufacturer's protocol. In brief, recombinant TOP1 protein was incubated with recombinant purified BET-proteins for 6 min in TOP1 assay buffer (10 mM Tris-HCl, pH 7.9, 1 mM EDTA, 150 mM NaCl, 0.1% BSA, 0.1 mM spermidine, 5% glycerol) on ice and then incubated with supercoiled pHOT-1 DNA at 37°C for 20 min. The reaction was terminated by STOP buffer (1% Sarkosyl, 0.25% bromophenol blue, 5% glycerol). Samples were electrophoresed on a 1% agarose gel in TAE buffer, and DNA was visualized using ethidium bromide (EtBr) stain.

In vitro acetylation assay

Recombinant PCAF protein and histone H2B were incubated with HAT assay buffer (50 mM Tris-HCl, pH 8.0, 50 mM NaCl, 4 mM $MgCl_2$, 0.1 mM EDTA, 1 mM DTT, 10% glycerol) in the presence or absence of Acetyl-CoA (Sigma). Input samples were subjected to SDS-PAGE and stained with Bio-Safe Coomassie G-250 (Bio-Rad). Acetylation was analyzed by western blotting with anti-histone H2B K120 acetylation antibody (Millipore, #07-564).

Statistical analysis

Graphs were created and statistics were calculated with Prism software (GraphPad). If the data were two groups, a two-tailed Student's t-test was used. One-way analysis of variance (ANOVA) was used when comparing more than two groups, followed by a Dunnett multiple comparison test. P-values and sample sizes are provided in figure legends. Experiments were repeated at least two times using biologically independent replicates with technical replicates as indicated, with exact experiment numbers indicated in the figure legends and methods.

Additional methods are described in Supplemental Materials and Methods.

Acknowledgments

References

Agarwal P, Miller KM. 2016. The nucleosome: orchestrating DNA damage signaling and repair within chromatin. *Biochem Cell Biol* **94:** 381–395. doi:10.1139/bcb-2016-0017

Andrieu G, Belkina AC, Denis GV. 2016. Clinical trials for BET inhibitors run ahead of the science. *Drug Discov Today Technol* **19:** 45–50. doi:10.1016/j.ddtec.2016.06.004

Arnoult N, Correia A, Ma J, Merlo A, Garcia-Gomez S, Maric M, Tognetti M, Benner CW, Boulton SJ, Saghatelian A, et al. 2017. Regulation of DNA repair pathway choice in S and G2 phases by the NHEJ inhibitor CYREN. *Nature* **549:** 548–552. doi:10.1038/nature24023

Aymard F, Bugler B, Schmidt CK, Guillou E, Caron P, Briois S, Iacovoni JS, Daburon V, Miller KM, Jackson SP, et al. 2014. Transcriptionally active chromatin recruits homologous recombination at DNA double-strand breaks. *Nat Struct Mol Biol* **21:** 366–374. doi:10.1038/nsmb.2796

Balasubramanyam K, Altaf M, Varier RA, Swaminathan V, Ravindran A, Sadhale PP, Kundu TK. 2004. Polyisoprenylated benzophenone, garcinol, a natural histone acetyltransferase inhibitor, represses chromatin transcription and alters global gene expression. *J Biol Chem* **279:** 33716–33726. doi:10.1074/jbc.M402839200

Baranello L, Wojtowicz D, Cui K, Devaiah BN, Chung HJ, Chan-Salis KY, Guha R, Wilson K, Zhang X, Zhang H, et al. 2016. RNA polymerase II regulates topoisomerase 1 activity to favor efficient transcription. *Cell* **165:** 357–371. doi:10.1016/j.cell.2016.02.036

Barbieri I, Cannizzaro E, Dawson MA. 2013. Bromodomains as therapeutic targets in cancer. *Brief Funct Genomics* **12:** 219–230. doi:10.1093/bfgp/elt007

Bennardo N, Cheng A, Huang N, Stark JM. 2008. Alternative-NHEJ is a mechanistically distinct pathway of mammalian

chromosome break repair. *PLoS Genet* **4:** e1000110. doi:10
.1371/journal.pgen.1000110

Bensaude O. 2011. Inhibiting eukaryotic transcription: Which
compound to choose? How to evaluate its activity? *Transcription* **2:** 103–108. doi:10.4161/trns.2.3.16172

Bhagwat AS, Roe JS, Mok BYL, Hohmann AF, Shi J, Vakoc CR.
2016. BET bromodomain inhibition releases the mediator
complex from select *cis*-regulatory elements. *Cell Rep* **15:**
519–530. doi:10.1016/j.celrep.2016.03.054

Bhatia V, Barroso SI, García-Rubio ML, Tumini E, Herrera-
Moyano E, Aguilera A. 2014. BRCA2 prevents R-loop accumu-
lation and associates with TREX-2 mRNA export factor
PCID2. *Nature* **511:** 362–365. doi:10.1038/nature13374

Boguslawski SJ, Smith DE, Michalak MA, Mickelson KE, Yehle
CO, Patterson WL, Carrico RJ. 1986. Characterization of
monoclonal antibody to DNA · RNA and its application to
immunodetection of hybrids. *J Immunol Methods* **89:** 123–
130. doi:10.1016/0022-1759(86)90040-2

Boi M, Gaudio E, Bonetti P, Kwee I, Bernasconi E, Tarantelli C,
Rinaldi A, Testoni M, Cascione L, Ponzoni M, et al. 2015.
The BET bromodomain inhibitor OTX015 affects pathogenet-
ic pathways in preclinical B-cell tumor models and synergizes
with targeted drugs. *Clin Cancer Res* **21:** 1628–1638. doi:10
.1158/1078-0432.CCR-14-1561

Bowry A, Piberger AL, Rojas P, Saponaro M, Petermann E. 2018.
BET inhibition induces HEXIM1- and RAD51-dependent con-
flicts between transcription and replication. *Cell Rep* **25:**
2061–2069.e4. doi:10.1016/j.celrep.2018.10.079

Bunch H, Lawney BP, Lin YF, Asaithamby A, Murshid A, Wang
YE, Chen BP, Calderwood SK. 2015. Transcriptional elonga-
tion requires DNA break-induced signalling. *Nat Commun*
6: 10191. doi:10.1038/ncomms10191

Canela A, Maman Y, Huang SN, Wutz G, Tang W, Zagnoli-Vieira
G, Callen E, Wong N, Day A, Peters JM, et al. 2019. Topoisom-
erase II-induced chromosome breakage and translocation is
determined by chromosome architecture and transcriptional
activity. *Mol Cell* **75:** 252–266.e8. doi:10.1016/j.molcel.2019
.04.030

Chen L, Chen JY, Zhang X, Gu Y, Xiao R, Shao C, Tang P, Qian H,
Luo D, Li H, et al. 2017. R-ChIP using inactive RNase H re-
veals dynamic coupling of R-loops with transcriptional paus-
ing at gene promoters. *Mol Cell* **68:** 745–757.e5. doi:10.1016/
j.molcel.2017.10.008

Chiang CM. 2009. Brd4 engagement from chromatin targeting to
transcriptional regulation: selective contact with acetylated
histone H3 and H4. *F1000 Biol Rep* **1:** 98.

Ciccia A, Elledge SJ. 2010. The DNA damage response: making it
safe to play with knives. *Mol Cell* **40:** 179–204. doi:10.1016/j
.molcel.2010.09.019

Classen S, Olland S, Berger JM. 2003. Structure of the topoisom-
erase II ATPase region and its mechanism of inhibition by the
chemotherapeutic agent ICRF-187. *Proc Natl Acad Sci* **100:**
10629–10634. doi:10.1073/pnas.1832879100

Clements A, Rojas JR, Trievel RC, Wang L, Berger SL, Marmor-
stein R. 1999. Crystal structure of the histone acetyltransfer-
ase domain of the human PCAF transcriptional regulator
bound to coenzyme A. *EMBO J* **18:** 3521–3532. doi:10.1093/
emboj/18.13.3521

Clouaire T, Rocher V, Lashgari A, Arnould C, Aguirrebengoa M,
Biernacka A, Skrzypczak M, Aymard F, Fongang B, Dojer N,
et al. 2018. Comprehensive mapping of histone modifications
at DNA double-strand breaks deciphers repair pathway chro-
matin signatures. *Mol Cell* **72:** 250–262.e6. doi:10.1016/j
.molcel.2018.08.020

Cortes Ledesma F, El Khamisy SF, Zuma MC, Osborn K, Calde-
cott KW. 2009. A human 5′-tyrosyl DNA phosphodiesterase
that repairs topoisomerase-mediated DNA damage. *Nature*
461: 674–678. doi:10.1038/nature08444

Crossley MP, Bocek M, Cimprich KA. 2019. R-loops as cellular
regulators and genomic threats. *Mol Cell* **73:** 398–411. doi:10
.1016/j.molcel.2019.01.024

Dawson MA, Prinjha RK, Dittmann A, Giotopoulos G, Bant-
scheff M, Chan WI, Robson SC, Chung CW, Hopf C, Savitski
MM, et al. 2011. Inhibition of BET recruitment to chromatin
as an effective treatment for MLL-fusion leukaemia. *Nature*
478: 529–533. doi:10.1038/nature10509

Densham RM, Morris JR. 2017. The BRCA1 ubiquitin ligase func-
tion sets a new trend for remodelling in DNA repair. *Nucleus*
8: 116–125. doi:10.1080/19491034.2016.1267092

Devaiah BN, Lewis BA, Cherman N, Hewitt MC, Albrecht BK,
Robey PG, Ozato K, Sims RJ III, Singer DS. 2012. BRD4 is an
atypical kinase that phosphorylates serine2 of the RNA poly-
merase II carboxy-terminal domain. *Proc Natl Acad Sci* **109:**
6927–6932. doi:10.1073/pnas.1120422109

Di Micco R, Fontanals-Cirera B, Low R, Ntziachristos P, Yuen SK,
Lovell CD, Dolgalev I, Yonekubo Y, Zhang G, Rusinova E,
et al. 2014. Control of embryonic stem cell identity by
BRD4-dependent transcriptional elongation of super-enhanc-
er-associated pluripotency genes. *Cell Rep* **9:** 234–247.
doi:10.1016/j.celrep.2014.08.055

Drolet M, Phoenix P, Menzel R, Masse E, Liu LF, Crouch RJ. 1995.
Overexpression of RNase H partially complements the
growth defect of an *Escherichia coli* δ topA mutant: R-loop
formation is a major problem in the absence of DNA topo-
isomerase I. *Proc Natl Acad Sci* **92:** 3526–3530. doi:10.1073/
pnas.92.8.3526

El Hage A, French SL, Beyer AL, Tollervey D. 2010. Loss of topo-
isomerase I leads to R-loop-mediated transcriptional blocks
during ribosomal RNA synthesis. *Genes Dev* **24:** 1546–1558.
doi:10.1101/gad.573310

Fenech M, Kirsch-Volders M, Natarajan AT, Surralles J, Crott JW,
Parry J, Norppa H, Eastmond DA, Tucker JD, Thomas P. 2011.
Molecular mechanisms of micronucleus, nucleoplasmic
bridge and nuclear bud formation in mammalian and human
cells. *Mutagenesis* **26:** 125–132. doi:10.1093/mutage/geq052

Fierz B, Chatterjee C, McGinty RK, Bar-Dagan M, Raleigh DP,
Muir TW. 2011. Histone H2B ubiquitylation disrupts local
and higher-order chromatin compaction. *Nat Chem Biol* **7:**
113–119. doi:10.1038/nchembio.501

Filippakopoulos P, Knapp S. 2012. The bromodomain interaction
module. *FEBS Lett* **586:** 2692–2704. doi:10.1016/j.febslet.2012
.04.045

Filippakopoulos P, Qi J, Picaud S, Shen Y, Smith WB, Fedorov O,
Morse EM, Keates T, Hickman TT, Felletar I, et al. 2010.
Selective inhibition of BET bromodomains. *Nature* **468:**
1067–1073. doi:10.1038/nature09504

Filippakopoulos P, Picaud S, Mangos M, Keates T, Lambert JP,
Barsyte-Lovejoy D, Felletar I, Volkmer R, Müller S, Pawson
T, et al. 2012. Histone recognition and large-scale structural
analysis of the human bromodomain family. *Cell* **149:** 214–
231. doi:10.1016/j.cell.2012.02.013

Floyd SR, Pacold ME, Huang Q, Clarke SM, Lam FC, Cannell IG,
Bryson BD, Rameseder J, Lee MJ, Blake EJ, et al. 2013. The bro-
modomain protein Brd4 insulates chromatin from DNA dam-
age signalling. *Nature* **498:** 246–250. doi:10.1038/nature12147

Fong CY, Gilan O, Lam EY, Rubin AF, Ftouni S, Tyler D, Stanley
K, Sinha D, Yeh P, Morison J, et al. 2015. BET inhibitor resis-
tance emerges from leukaemia stem cells. *Nature* **525:** 538–
542. doi:10.1038/nature14888

Fradet-Turcotte A, Canny MD, Escribano-Díaz C, Orthwein A, Leung CC, Huang H, Landry MC, Kitevski-LeBlanc J, Noordermeer SM, Sicheri F, et al. 2013. 53BP1 is a reader of the DNA-damage-induced H2A Lys 15 ubiquitin mark. *Nature* **499:** 50–54. doi:10.1038/nature12318

Fujisawa T, Filippakopoulos P. 2017. Functions of bromodomain-containing proteins and their roles in homeostasis and cancer. *Nat Rev Mol Cell Biol* **18:** 246–262. doi:10.1038/nrm.2016.143

Gaillard H, Aguilera A. 2016. Transcription as a threat to genome integrity. *Annu Rev Biochem* **85:** 291–317. doi:10.1146/annurev-biochem-060815-014908

Giurgiu M, Reinhard J, Brauner B, Dunger-Kaltenbach I, Fobo G, Frishman G, Montrone C, Ruepp A. 2019. CORUM: the comprehensive resource of mammalian protein complexes—2019. *Nucleic Acids Res* **47:** D559–D563. doi:10.1093/nar/gky973

Gong F, Miller KM. 2013. Mammalian DNA repair: HATs and HDACs make their mark through histone acetylation. *Mutat Res* **750:** 23–30. doi:10.1016/j.mrfmmm.2013.07.002

Gong F, Chiu LY, Cox B, Aymard F, Clouaire T, Leung JW, Cammarata M, Perez M, Agarwal P, Brodbelt JS, et al. 2015. Screen identifies bromodomain protein ZMYND8 in chromatin recognition of transcription-associated DNA damage that promotes homologous recombination. *Genes Dev* **29:** 197–211. doi:10.1101/gad.252189.114

Gong F, Chiu LY, Miller KM. 2016. Acetylation reader proteins: linking acetylation signaling to genome maintenance and cancer. *PLoS Genet* **12:** e1006272. doi:10.1371/journal.pgen.1006272

Haffner MC, Aryee MJ, Toubaji A, Esopi DM, Albadine R, Gurel B, Isaacs WB, Bova GS, Liu W, Xu J, et al. 2010. Androgen-induced TOP2B-mediated double-strand breaks and prostate cancer gene rearrangements. *Nat Genet* **42:** 668–675. doi:10.1038/ng.613

Hamperl S, Bocek MJ, Saldivar JC, Swigut T, Cimprich KA. 2017. Transcription-replication conflict orientation modulates R-loop levels and activates distinct DNA damage responses. *Cell* **170:** 774–786.e19. doi:10.1016/j.cell.2017.07.043

Hatchi E, Skourti-Stathaki K, Ventz S, Pinello L, Yen A, Kamieniarz-Gdula K, Dimitrov S, Pathania S, McKinney KM, Eaton ML, et al. 2015. BRCA1 recruitment to transcriptional pause sites is required for R-loop-driven DNA damage repair. *Mol Cell* **57:** 636–647. doi:10.1016/j.molcel.2015.01.011

Helmlinger D, Tora L. 2017. Sharing the SAGA. *Trends Biochem Sci* **42:** 850–861. doi:10.1016/j.tibs.2017.09.001

Hu Z, Zhang A, Storz G, Gottesman S, Leppla SH. 2006. An antibody-based microarray assay for small RNA detection. *Nucleic Acids Res* **34:** e52. doi:10.1093/nar/gkl142

Huertas P, Aguilera A. 2003. Cotranscriptionally formed DNA: RNA hybrids mediate transcription elongation impairment and transcription-associated recombination. *Mol Cell* **12:** 711–721. doi:10.1016/j.molcel.2003.08.010

Humphreys PG, Bamborough P, Chung CW, Craggs PD, Gordon L, Grandi P, Hayhow TG, Hussain J, Jones KL, Lindon M, et al. 2017. Discovery of a potent, cell penetrant, and selective p300/CBP-associated factor (PCAF)/general control nonderepressible 5 (GCN5) bromodomain chemical probe. *J Med Chem* **60:** 695–709. doi:10.1021/acs.jmedchem.6b01566

Ikura T, Ogryzko VV, Grigoriev M, Groisman R, Wang J, Horikoshi M, Scully R, Qin J, Nakatani Y. 2000. Involvement of the TIP60 histone acetylase complex in DNA repair and apoptosis. *Cell* **102:** 463–473. doi:10.1016/S0092-8674(00)00051-9

Jackson SP, Bartek J. 2009. The DNA-damage response in human biology and disease. *Nature* **461:** 1071–1078. doi:10.1038/nature08467

Jackson SP, Durocher D. 2013. Regulation of DNA damage responses by ubiquitin and SUMO. *Mol Cell* **49:** 795–807. doi:10.1016/j.molcel.2013.01.017

Jang MK, Mochizuki K, Zhou M, Jeong HS, Brady JN, Ozato K. 2005. The bromodomain protein Brd4 is a positive regulatory component of P-TEFb and stimulates RNA polymerase II-dependent transcription. *Mol Cell* **19:** 523–534. doi:10.1016/j.molcel.2005.06.027

Ju BG, Lunyak VV, Perissi V, Garcia-Bassets I, Rose DW, Glass CK, Rosenfeld MG. 2006. A topoisomerase IIβ-mediated dsDNA break required for regulated transcription. *Science* **312:** 1798–1802. doi:10.1126/science.1127196

Karakashev S, Zhu H, Yokoyama Y, Zhao B, Fatkhutdinov N, Kossenkov AV, Wilson AJ, Simpkins F, Speicher D, Khabele D, et al. 2017. BET bromodomain inhibition synergizes with PARP inhibitor in epithelial ovarian cancer. *Cell Rep* **21:** 3398–3405. doi:10.1016/j.celrep.2017.11.095

Khurana S, Kruhlak MJ, Kim J, Tran AD, Liu J, Nyswaner K, Shi L, Jailwala P, Sung MH, Hakim O, et al. 2014. A macrohistone variant links dynamic chromatin compaction to BRCA1-dependent genome maintenance. *Cell Rep* **8:** 1049–1062. doi:10.1016/j.celrep.2014.07.024

Kim JJ, Lee SY, Miller KM. 2019. Preserving genome integrity and function: the DNA damage response and histone modifications. *Crit Rev Biochem Mol Biol* **54:** 208–241. doi:10.1080/10409238.2019.1620676

Lahusen TJ, Kim SJ, Miao K, Huang Z, Xu X, Deng CX. 2018. BRCA1 function in the intra-S checkpoint is activated by acetylation via a pCAF/SIRT1 axis. *Oncogene* **37:** 2343–2350. doi:10.1038/s41388-018-0127-1

Lambert JP, Picaud S, Fujisawa T, Hou H, Savitsky P, Uusküla-Reimand L, Gupta GD, Abdouni H, Lin ZY, Tucholska M, et al. 2019. Interactome rewiring following pharmacological targeting of BET bromodomains. *Mol Cell* **73:** 621–638.e17. doi:10.1016/j.molcel.2018.11.006

Lee KK, Workman JL. 2007. Histone acetyltransferase complexes: one size doesn't fit all. *Nat Rev Mol Cell Biol* **8:** 284–295. doi:10.1038/nrm2145

Leung JW, Makharashvili N, Agarwal P, Chiu LY, Pourpre R, Cammarata MB, Cannon JR, Sherker A, Durocher D, Brodbelt JS, et al. 2017. ZMYM3 regulates BRCA1 localization at damaged chromatin to promote DNA repair. *Genes Dev* **31:** 260–274. doi:10.1101/gad.292516.116

Li M, Pokharel S, Wang JT, Xu X, Liu Y. 2015. RECQ5-dependent SUMOylation of DNA topoisomerase I prevents transcription-associated genome instability. *Nat Commun* **6:** 6720. doi:10.1038/ncomms7720

Li X, Baek G, Ramanand SG, Sharp A, Gao Y, Yuan W, Welti J, Rodrigues DN, Dolling D, Figueiredo I, et al. 2018. BRD4 promotes DNA repair and mediates the formation of TMPRSS2-ERG gene rearrangements in prostate cancer. *Cell Rep* **22:** 796–808. doi:10.1016/j.celrep.2017.12.078

Lukas J, Lukas C, Bartek J. 2011. More than just a focus: the chromatin response to DNA damage and its role in genome integrity maintenance. *Nat Cell Biol* **13:** 1161–1169. doi:10.1038/ncb2344

Madabhushi R, Gao F, Pfenning AR, Pan L, Yamakawa S, Seo J, Rueda R, Phan TX, Yamakawa H, Pao PC, et al. 2015. Activity-induced DNA breaks govern the expression of neuronal early-response genes. *Cell* **161:** 1592–1605. doi:10.1016/j.cell.2015.05.032

Makharashvili N, Arora S, Yin Y, Fu Q, Wen X, Lee JH, Kao CH, Leung JW, Miller KM, Paull TT. 2018. Sae2/CtIP prevents R-loop accumulation in eukaryotic cells. *Elife* **7**. doi:10.7554/eLife.42733

Manzo SG, Hartono SR, Sanz LA, Marinello J, De Biasi S, Cossarizza A, Capranico G, Chedin F. 2018. DNA Topoisomerase I differentially modulates R-loops across the human genome. *Genome Biol* **19:** 100. doi:10.1186/s13059-018-1478-1

Mao Y, Desai SD, Ting CY, Hwang J, Liu LF. 2001. 26 S proteasome-mediated degradation of topoisomerase II cleavable complexes. *J Biol Chem* **276:** 40652–40658. doi:10.1074/jbc .M104009200

Marnef A, Cohen S, Legube G. 2017. Transcription-coupled DNA double-strand break repair: active genes need special care. *J Mol Biol* **429:** 1277–1288. doi:10.1016/j.jmb.2017.03.024

Massé E, Phoenix P, Drolet M. 1997. DNA topoisomerases regulate R-loop formation during transcription of the *rrnB* operon in *Escherichia coli*. *J Biol Chem* **272:** 12816–12823. doi:10 .1074/jbc.272.19.12816

Meldal BH, Forner-Martinez O, Costanzo MC, Dana J, Demeter J, Dumousseau M, Dwight SS, Gaulton A, Licata L, Melidoni AN, et al. 2015. The complex portal—an encyclopaedia of macromolecular complexes. *Nucleic Acids Res* **43:** D479–D484. doi:10.1093/nar/gku975

Miller KM, Jackson SP. 2012. Histone marks: repairing DNA breaks within the context of chromatin. *Biochem Soc Trans* **40:** 370–376. doi:10.1042/BST20110747

Miller KM, Tjeertes JV, Coates J, Legube G, Polo SE, Britton S, Jackson SP. 2010. Human HDAC1 and HDAC2 function in the DNA-damage response to promote DNA nonhomologous end-joining. *Nat Struct Mol Biol* **17:** 1144–1151. doi:10.1038/ nsmb.1899

Muller S, Filippakopoulos P, Knapp S. 2011. Bromodomains as therapeutic targets. *Expert Rev Mol Med* **13:** e29. doi:10 .1017/S1462399411001992

Musselman CA, Lalonde ME, Côté J, Kutateladze TG. 2012. Perceiving the epigenetic landscape through histone readers. *Nat Struct Mol Biol* **19:** 1218–1227. doi:10.1038/nsmb.2436

Nagy Z, Tora L. 2007. Distinct GCN5/PCAF-containing complexes function as co-activators and are involved in transcription factor and global histone acetylation. *Oncogene* **26:** 5341–5357. doi:10.1038/sj.onc.1210604

Negrini S, Gorgoulis VG, Halazonetis TD. 2010. Genomic instability—an evolving hallmark of cancer. *Nat Rev Mol Cell Biol* **11:** 220–228. doi:10.1038/nrm2858

Oberdoerffer P. 2015. Stop relaxing: how DNA damage-induced chromatin compaction may affect epigenetic integrity and disease. *Mol Cell Oncol* **2:** e970952. doi:10.4161/23723548 .2014.970952

Panier S, Boulton SJ. 2014. Double-strand break repair: 53BP1 comes into focus. *Nat Rev Mol Cell Biol* **15:** 7–18. doi:10 .1038/nrm3719

Patel MC, Debrosse M, Smith M, Dey A, Huynh W, Sarai N, Heightman TD, Tamura T, Ozato K. 2013. BRD4 coordinates recruitment of pause release factor P-TEFb and the pausing complex NELF/DSIF to regulate transcription elongation of interferon-stimulated genes. *Mol Cell Biol* **33:** 2497–2507. doi:10.1128/MCB.01180-12

Pierce AJ, Johnson RD, Thompson LH, Jasin M. 1999. XRCC3 promotes homology-directed repair of DNA damage in mammalian cells. *Genes Dev* **13:** 2633–2638. doi:10.1101/gad.13 .20.2633

Pinder J, Salsman J, Dellaire G. 2015. Nuclear domain 'knock-in' screen for the evaluation and identification of small molecule enhancers of CRISPR-based genome editing. *Nucleic Acids Res* **43:** 9379–9392. doi:10.1093/nar/gkv993

Pohjoismäki JL, Holmes JB, Wood SR, Yang MY, Yasukawa T, Reyes A, Bailey LJ, Cluett TJ, Goffart S, Willcox S, et al. 2010. Mammalian mitochondrial DNA replication intermedi-

ates are essentially duplex but contain extensive tracts of RNA/DNA hybrid. *J Mol Biol* **397:** 1144–1155. doi:10.1016/j .jmb.2010.02.029

Polo SE, Jackson SP. 2011. Dynamics of DNA damage response proteins at DNA breaks: a focus on protein modifications. *Genes Dev* **25:** 409–433. doi:10.1101/gad.2021311

Puget N, Miller KM, Legube G. 2019. Non-canonical DNA/RNA structures during transcription-coupled double-strand break repair: roadblocks or *bona fide* repair intermediates? *DNA Repair (Amst)* **81:** 102661. doi:10.1016/j.dnarep.2019.102661

Ramachandran S, Haddad D, Li C, Le MX, Ling AK, So CC, Nepal RM, Gommerman JL, Yu K, Ketela T, et al. 2016. The SAGA deubiquitination module promotes DNA repair and class switch recombination through ATM and DNAPK-mediated γH2AX formation. *Cell Rep* **15:** 1554–1565. doi:10.1016/j .celrep.2016.04.041

Ray Chaudhuri A, Nussenzweig A. 2017. The multifaceted roles of PARP1 in DNA repair and chromatin remodelling. *Nat Rev Mol Cell Biol* **18:** 610–621. doi:10.1038/nrm.2017.53

Roberts B, Haupt A, Tucker A, Grancharova T, Arakaki J, Fuqua MA, Nelson A, Hookway C, Ludmann SA, Mueller IA, et al. 2017. Systematic gene tagging using CRISPR/Cas9 in human stem cells to illuminate cell organization. *Mol Biol Cell* **28:** 2854–2874. doi:10.1091/mbc.e17-03-0209

Scully R, Xie A. 2013. Double strand break repair functions of histone H2AX. *Mutat Res* **750:** 5–14. doi:10.1016/j.mrfmmm .2013.07.007

Seto E, Yoshida M. 2014. Erasers of histone acetylation: the histone deacetylase enzymes. *Cold Spring Harb Perspect Biol* **6:** a018713. doi:10.1101/cshperspect.a018713

Shanbhag NM, Rafalska-Metcalf IU, Balane-Bolivar C, Janicki SM, Greenberg RA. 2010. ATM-dependent chromatin changes silence transcription in *cis* to DNA double-strand breaks. *Cell* **141:** 970–981. doi:10.1016/j.cell.2010.04.038

Shivji MKK, Renaudin X, Williams CH, Venkitaraman AR. 2018. BRCA2 regulates transcription elongation by RNA polymerase II to prevent R-loop accumulation. *Cell Rep* **22:** 1031–1039. doi:10.1016/j.celrep.2017.12.086

Skourti-Stathaki K, Kamieniarz-Gdula K, Proudfoot NJ. 2014. R-loops induce repressive chromatin marks over mammalian gene terminators. *Nature* **516:** 436–439. doi:10.1038/ nature13787

Sollier J, Cimprich KA. 2015. Breaking bad: R-loops and genome integrity. *Trends Cell Biol* **25:** 514–522. doi:10.1016/j.tcb .2015.05.003

Sollier J, Stork CT, García-Rubio ML, Paulsen RD, Aguilera A, Cimprich KA. 2014. Transcription-coupled nucleotide excision repair factors promote R-loop-induced genome instability. *Mol Cell* **56:** 777–785. doi:10.1016/j.molcel.2014.10.020

Stathis A, Bertoni F. 2018. BET proteins as targets for anticancer treatment. *Cancer Discov* **8:** 24–36. doi:10.1158/2159-8290 .CD-17-0605

Stolz R, Sulthana S, Hartono SR, Malig M, Benham CJ, Chedin F. 2019. Interplay between DNA sequence and negative superhelicity drives R-loop structures. *Proc Natl Acad Sci* **116:** 6260–6269. doi:10.1073/pnas.1819476116

Stork CT, Bocek M, Crossley MP, Sollier J, Sanz LA, Chédin F, Swigut T, Cimprich KA. 2016. Co-transcriptional R-loops are the main cause of estrogen-induced DNA damage. *Elife* **5.** doi:10.7554/eLife.17548

Sun C, Yin J, Fang Y, Chen J, Jeong KJ, Chen X, Vellano CP, Ju Z, Zhao W, Zhang D, et al. 2018. BRD4 inhibition is synthetic lethal with PARP inhibitors through the induction of homologous recombination deficiency. *Cancer Cell* **33:** 401–416.e8. doi:10.1016/j.ccell.2018.01.019

Tang J, Cho NW, Cui G, Manion EM, Shanbhag NM, Botuyan MV, Mer G, Greenberg RA. 2013. Acetylation limits 53BP1 association with damaged chromatin to promote homologous recombination. *Nat Struct Mol Biol* **20:** 317–325. doi:10.1038/nsmb.2499

Teo G, Liu G, Zhang J, Nesvizhskii AI, Gingras AC, Choi H. 2014. SAINTexpress: improvements and additional features in significance analysis of INTeractome software. *J Proteomics* **100:** 37–43. doi:10.1016/j.jprot.2013.10.023

Tubbs A, Nussenzweig A. 2017. Endogenous DNA damage as a source of genomic instability in cancer. *Cell* **168:** 644–656. doi:10.1016/j.cell.2017.01.002

Tuduri S, Crabbé L, Conti C, Tourrière H, Holtgreve-Grez H, Jauch A, Pantesco V, De Vos J, Thomas A, Theillet C, et al. 2009. Topoisomerase I suppresses genomic instability by preventing interference between replication and transcription. *Nat Cell Biol* **11:** 1315–1324. doi:10.1038/ncb1984

Verdin E, Ott M. 2015. 50 years of protein acetylation: from gene regulation to epigenetics, metabolism and beyond. *Nat Rev Mol Cell Biol* **16:** 258–264. doi:10.1038/nrm3931

Wu SY, Chiang CM. 2007. The double bromodomain-containing chromatin adaptor Brd4 and transcriptional regulation. *J Biol Chem* **282:** 13141–13145. doi:10.1074/jbc.R700001200

Wu L, Li L, Zhou B, Qin Z, Dou Y. 2014. H2B ubiquitylation promotes RNA Pol II processivity via PAF1 and pTEFb. *Mol Cell* **54:** 920–931. doi:10.1016/j.molcel.2014.04.013

Wysocka J, Reilly PT, Herr W. 2001. Loss of HCF-1–chromatin association precedes temperature-induced growth arrest of tsBN67 cells. *Mol Cell Biol* **21:** 3820–3829. doi:10.1128/MCB.21.11.3820-3829.2001

Xia J, Chiu LY, Nehring RB, Bravo Núñez MA, Mei Q, Perez M, Zhai Y, Fitzgerald DM, Pribis JP, Wang Y, et al. 2019. Bacteria-to-human protein networks reveal origins of endogenous DNA damage. *Cell* **176:** 127–143.e24. doi:10.1016/j.cell.2018.12.008

Xiao T, Kao CF, Krogan NJ, Sun ZW, Greenblatt JF, Osley MA, Strahl BD. 2005. Histone H2B ubiquitylation is associated with elongating RNA polymerase II. *Mol Cell Biol* **25:** 637–651. doi:10.1128/MCB.25.2.637-651.2005

Yang Z, Yik JH, Chen R, He N, Jang MK, Ozato K, Zhou Q. 2005. Recruitment of P-TEFb for stimulation of transcriptional elongation by the bromodomain protein Brd4. *Mol Cell* **19:** 535–545. doi:10.1016/j.molcel.2005.06.029

Zhang G, Smith SG, Zhou MM. 2015. Discovery of chemical inhibitors of human bromodomains. *Chem Rev* **115:** 11625–11668. doi:10.1021/acs.chemrev.5b00205

Zhang X, Chiang HC, Wang Y, Zhang C, Smith S, Zhao X, Nair SJ, Michalek J, Jatoi I, Lautner M, et al. 2017. Attenuation of RNA polymerase II pausing mitigates BRCA1-associated R-loop accumulation and tumorigenesis. *Nat Commun* **8:** 15908. doi:10.1038/ncomms15908

Zhao Y, Lang G, Ito S, Bonnet J, Metzger E, Sawatsubashi S, Suzuki E, Le Guezennec X, Stunnenberg HG, Krasnov A, et al. 2008. A TFTC/STAGA module mediates histone H2A and H2B deubiquitination, coactivates nuclear receptors, and counteracts heterochromatin silencing. *Mol Cell* **29:** 92–101. doi:10.1016/j.molcel.2007.12.011

Zhao M, Geng R, Guo X, Yuan R, Zhou X, Zhong Y, Huo Y, Zhou M, Shen Q, Li Y, et al. 2017. PCAF/GCN5-mediated acetylation of RPA1 promotes nucleotide excision repair. *Cell Rep* **20:** 1997–2009. doi:10.1016/j.celrep.2017.08.015

Systematic bromodomain protein screens identify homologous recombination and R-loop suppression pathways involved in genome integrity

Jae Jin Kim, Seo Yun Lee, Fade Gong, et al.

Supplemental Material	http://genesdev.cshlp.org/content/suppl/2019/11/20/gad.331231.119.DC1
	Published online November 21, 2019 in advance of the full issue.
Creative Commons License	This article is distributed exclusively by Cold Spring Harbor Laboratory Press for the first six months after the full-issue publication date (see http://genesdev.cshlp.org/site/misc/terms.xhtml). After six months, it is available under a Creative Commons License (Attribution-NonCommercial 4.0 International), as described at http://creativecommons.org/licenses/by-nc/4.0/.
Email Alerting Service	Receive free email alerts when new articles cite this article - sign up in the box at the top right corner of the article or **click here.**